WL-TR-95-3090

STRUCTURAL INTEGRITY ANALYSIS AND VERIFICATION OF AIRCRAFT STRUCTURES

K.L. Boyd, D.A. Jansen, S. Krishnan
Analytical Services and Materials, Inc.
107 Research Drive
Hampton, Virginia 23666

J.A. Harter
WL/FIBEC
2130 Eight Street, Suite 1
Wright-Patterson AFB, OH 45433-7542

Vol. I: Characterization of 7075-T7351 Aluminum; MODGRO Verification; MODGRO GUI Development

Final Report for Period 01 Oct - 31 Dec 1994

January 1996

Approved for public release; distribution is unlimited

FLIGHT DYNAMICS DIRECTORATE
WRIGHT LABORATORY
AIR FORCE MATERIEL COMMAND
WRIGHT-PATTERSON AFB, OHIO 45433-7542

NOTICE

When Government drawings, specifications, or other data are used for any purpose other than in connection with a definitely Government-related procurement, the United States Government incurs no responsibility or any obligation whatsoever. The fact that the government may have formulated or in any way supplied the said drawings, specifications, or other data, is not to be regarded by implication, or otherwise in any manner construed, as licensing the holder, or any other person or corporation; or as conveying any rights or permission to manufacture, use, or sell any patented invention that may in any way be related thereto.

This report is releasable to the National Technical Information Service (NTIS). At NTIS, it will be available to the general public, including foreign nations.

This technical report has been reviewed and is approved for publication.

JAMES A. HARTER
Aerospace Engineer
Fatigue, Fracture & Reliability Section
Structural Integrity Branch

KENNETH B. LEGER
Acting Tech Manager
Fatigue, Fracture & Reliability Sec
Structural Integrity Branch

JEROME PEARSON, Chief
Structural Integrity Branch
Structures Division

If your address has changed, if you wish to be removed from our mailing list, or if the addressee is no longer employed by your organization please notify WL/FIBEC , WPAFB, OH 45433-7542 to help us maintain a current mailing list.

Copies of this report should not be returned unless return is required by security considerations, contractual obligations, or notice on a specific document.

REPORT DOCUMENTATION PAGE

Form Approved
OMB No. 0704-0188

1. AGENCY USE ONLY *(Leave blank)*	2. REPORT DATE	3. REPORT TYPE AND DATES COVERED
	June 1995	Final, 1 Oct 94 to 31 Dec 94

4. TITLE AND SUBTITLE
Structural Integrity Analysis and Verification for Aircraft Structures - Vol. 1: Characterization of 7075-T7351 Aluminum; MODGRO Verficiation; MODGRO GUI Development

5. FUNDING NUMBERS
C: F33615-94-D-3212
PE: JMF573
PR: 2401
TA: 01
WU: 01

6. AUTHOR(S)
K. L. Boyd, D. A. Jansen, S. Krishnan, and J. A. Harter

7. PERFORMING ORGANIZATION NAME(S) AND ADDRESS(ES)
Analytical Services and Materials
107 Research Drive
Hampton VA 23666

8. PERFORMING ORGANIZATION REPORT NUMBER

9. SPONSORING / MONITORING AGENCY NAME(S) AND ADDRESS(ES)
Structural Integrity Branch (WL/FIBE)
FLIGHT DYNAMICS DIRECTORATE, WRIGHT LABORATORY
AIR FORCE MATERIEL COMMAND
Wright-Patterson AFB OH 45433-7542

10. SPONSORING / MONITORING AGENCY REPORT NUMBER
WL-TR-95-3090

11. SUPPLEMENTARY NOTES

12a. DISTRIBUTION / AVAILABILITY STATEMENT
Approved for public release; distribution is unlimited

12b. DISTRIBUTION CODE

13. ABSTRACT *(Maximum 200 words)*
Crack growth rate tests were performed for 7075-T7351 aluminum under standard laboratory environment. These data served to establish the baseline material properties of the alloy. The Air Force crack growth life prediction software (MODGRO) was used to predict the life of 7075-T7351 aluminum specimens tested with cracks emanating from open and pin loaded fastener holes. The ability to use cyclic material property data under any environment was added to MODGRO. The effect of cold-working and interference fit fasteners was also examined. In addition, a user-friendly graphical user interface (GUI) was added to MODGRO and is documented in this report.

14. SUBJECT TERMS
Fatigue Crack Growth, Coldworking, Interference Fit Fastener, MODGRO, Graphical User Interface

15. NUMBER OF PAGES
67

16. PRICE CODE

17. SECURITY CLASSIFICATION OF REPORT	18. SECURITY CLASSIFICATION OF THIS PAGE	19. SECURITY CLASSIFICATION OF ABSTRACT	20. LIMITATION OF ABSTRACT
Unclassified	Unclassified	Unclassified	UL

NSN 7540-01-280-5500

Standard Form 298 (Rev. 2-89)
Prescribed by ANSI Std. Z39-18
298-102

TABLE OF CONTENTS

LIST OF FIGURES

LIST OF TABLES

FOREWORD

This report was prepared by Analytical Services & Materials, Inc., Hampton Virginia for the Structural Integrity Branch, Fatigue, Fracture and Reliability Section (WL/FIBEC), Wright-Patterson Air Force Base, Ohio under contract F33615-94-D-3212," Structural Integrity Analysis and Verification for Aircraft Structures." The contract monitor was James A. Harter, WL/FIBEC. The period of performance for this report was October 1994 through December 1994.

The work performed under report (Delivery Order 0001) was performed by Analytical Services & Materials, Inc. personnel located at the WL/FIBE Fatigue & Fracture Test Facility, Bldg. 65, Area B, Wright-Patterson AFB, OH. The Principal Investigator and author of this report was Kevin L. Boyd. Technical inputs were submitted by Messrs. James A. Harter, Daniel A. Jansen and Srinivas Krishnan.

1. INTRODUCTION

This purpose of this research was to characterize the fatigue-crack-growth (FCGR) behavior of 7075-T73 aluminum and add a capability to model environmental effects (temperature, humidity, atmosphere, prior corrosion, chemical agents, etc.) in the MODGRO FCGR life prediction program. The data generated under this Delivery Order was developed under laboratory air environments, and served as baseline crack-growth material data for the specified material. It is anticipated that additional testing of this material, subjected to various environments, will be performed to adequately substantiate this capability.

It is important that testing be performed under controlled, laboratory conditions in order to quantify the degradation of material behavior due to the influence of various environmental factors. It is anticipated that the baseline data generated and analytical studies performed in this report will aid in the understanding of environmental effects on the FCGR behavior of this aluminum alloy. The final result of this effort will be the development of a method to incorporate the effects of various environments on the FCGR behavior of the 7075-T73 aluminum alloy. This method will be incorporated into the MODGRO program for the intent of making future life predictions of metallic materials exposed to different environments. A "user-friendly" Graphical User Interface (GUI) was added to expedite the usage of the computer program among US Air Force Air Logistics

Centers (ALC's) and government agencies, as well as enhancing the transition of this technology to industry.

This report will summarize the tasks performed under Delivery Order 0001 that contributed toward the achievement of the final results stated above.

2. EXECUTIVE SUMMARY

The objective of this research was to perform stress intensity factor modeling, crack-growth life predictions, verification testing, and develop a graphical user interface (GUI) for the crack-growth computer program, MODGRO [1]. This research was broken down into three major activities: stress intensity factor modeling and life predictions, verification testing, and Graphical User Interface (GUI) development. The entire program consisted of ten tasks.

The stress intensity factor modeling and life prediction activity consisted of three of the ten tasks; In Task 1, the numerical determination of mode I and II stress intensity factors was made for cracks propagating from an open-hole specimen. In Task 2, numerical determinations of the stress field around an open hole were made for both interference-fit and cold-worked fastener holes in a reverse-dog-bone specimen. In Task 3, the fatigue-crack-growth life predictions were made for all flawed specimen configurations in the verification testing.

The verification testing consisted of four of the ten tasks. In Tasks 4 and 5, flawed and open-hole specimen configurations of two different thicknesses were tested at different maximum stress levels. In Tasks 6 and 7, flawed and unflawed reverse-dog-bone

specimens were tested under various levels of interference (interference-fit fasteners and cold-working with fasteners).

The Graphical User Interface (GUI) development consisted of the last three of the ten tasks. In Task 8, the integration of menu buttons and dialogs to replace existing menu choices was completed. In Task 9, graphical, initial geometry and crack display options were developed for MODGRO. In Task 10, the MODGRO enhancements and program debugging operations were performed.

The enhancements to the existing crack growth life prediction code will be available in MODGRO Version 3.0. A MODGRO User's Manual will also be available in 1996. The User's Manual will summarize the capabilities, limitations, and assumptions made in creating the computer program. Examples of input and output screens will be provided to give an engineer a "feel" for the capabilities of the program. In addition to the User's Manual, on-line help will be available within the MODGRO program.

3. STRESS INTENSITY FACTOR MODELING AND LIFE PREDICTIONS

3.1. Specimen Stress Intensity/Residual Stress Modeling

Mode I and mode II stress intensity factor calculations were made for a specimen geometry possessing four radial cracks propagating from the maximum shear stress locations of an open hole in a finite width plate. The FRANC2D/L (FRacture ANalysis Code for Two-Dimensional, Layered Structures) [2] was used to calculate the stress intensity factors of the form:

$$K = \sigma_\infty \sqrt{\pi c}\, \beta_n \qquad (1)$$

where:

σ_∞ = ***remote stress***

c = ***crack length, width direction***

$\beta_n = f\,(loading, geometry)$

and

loading = Mode I, Mode II

geometry = specimen configuration, width, thickness

The FRANC2D/L code has automatic mesh generation capabilities, and allows the determination of stress intensity factors at different crack lengths, allowing for the development of curve fits to describe the crack length vs. stress intensity factor behavior. FRANC2D/L uses the maximum normal stress theory (mode II=0) to predict the direction of fatigue crack propagation [3]. FRANC2D/L may be used to model two-dimensional planar and layered structures.

The open-hole geometry was a 0.25-inch-diameter hole, centered in a 3.95 inch-wide by 16.0-inch-long plate, represented by the finite element geometry shown in Figure A.1 (Appendix A). The initial crack configuration consisted of four through cracks emanating radially from the hole at the locations of maximum shear stress. The initial crack length was 0.03 inches and transversed the entire thickness. The FRANC2D/L code was used to model one-half of the geometry (symmetry conditions were used along the Y-axis, see Figure A.2, Appendix A). The stress intensity factor was calculated for the initial crack length and a convergence study was performed to ensure that the stress intensity factor error was less than 1%. The convergence study established the minimum element size and mesh density required for an accurate solution, and this level of mesh refinement was maintained throughout the analysis. The crack growth increment size was based on the gradient of the crack length vs. stress intensity factor curve (i.e., the steeper the gradient, the smaller the increment). Typically, the increment size was 0.01 inches. The model was changed to two cracks propagating from opposite sides of the hole when the analysis predicted that the cracks had turned perpendicular to the direction of loading. The same symmetry conditions were used to reduce the degrees of freedom in the model. The analysis continued adding increments of crack length until the crack had grown through 80-90% of the specimen width. Test results verified that the critical crack size in these experiments occurred at values much less than this geometric constraint.

The results of the analysis can be found in Figure 1. Figure 1 contains the mode I stress normalized stress intensity factor as a function of crack length. The normalized stress intensity factor can easily be found by solving equation (1) for β_n. A table, containing these values, calculated values of $\mathbf{K_I}$ and $\mathbf{K_{II}}$, and the crack tip location (x- and y-coordinates) for each crack increment can be found in Table B.1 (Appendix B).

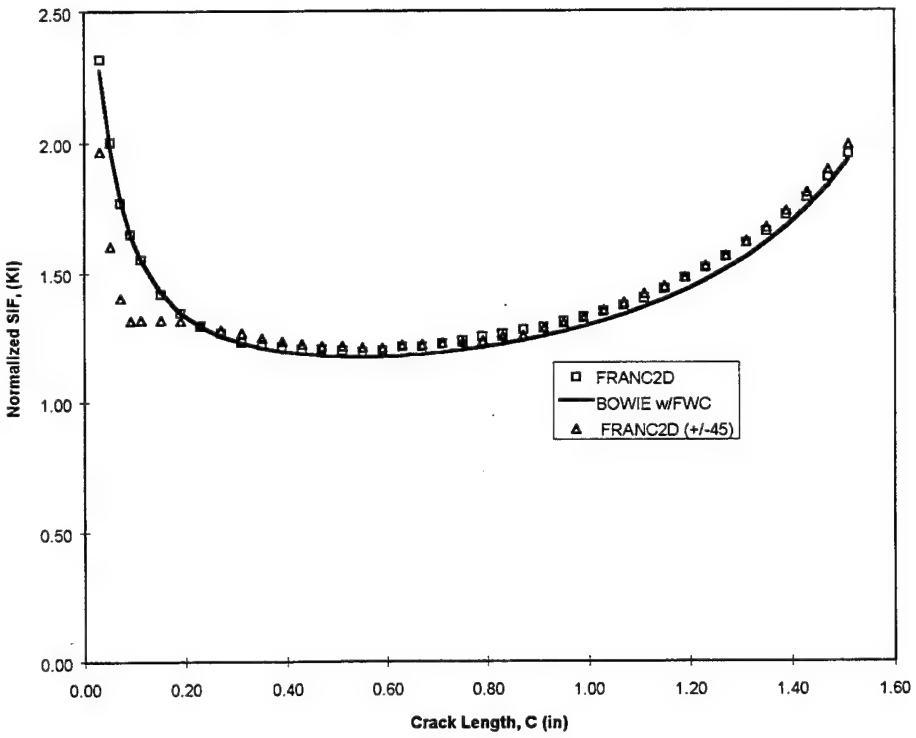

Figure 1 Comparison of Normalized Stress Intensity Factors

In Figure 1, the normalized stress intensity factors (K_I) for the geometry of interest (four cracks emanating at (+/-45) degrees form an open hole) is plotted against the standard Bowie solution for two through-cracks emanating form either side of an open hole [4].

Also, the classic Bowie solution case was analyzed using FRANC2D/L (FRANC2D) to evaluate the integrity of the finite element model and is shown in Figure 1. The error between the two classic cases was approximately 0-3%. The Bowie solution was approximated with a least squares curve fit using tabularized data [5]. In addition, this solution was modified with a finite width correction (Bowie w/FWC) [6]. This basic engineering approximation has been used successfully in the past and can be found elsewhere [7].

In order to compare the three solutions the crack length, c, for the (+/-45) degree case was represented by an "effective" c, that was calculated using the x-component of the crack length perpendicular to the direction of loading. All of the data that had x-component values less than the hole radius was neglected. This was necessary in order to take advantage of the standard **K** (stress intensity) solutions in MODGRO. Any differences could then be accounted for using the "Beta Correction" feature in MODGRO, if desired. The data "inflection" seen in the FRANC2D/L (+/-45) case is the point at which one of the cracks was arrested. This can be explained by the reduced stiffness ($\alpha\sigma$) in the vicinity of the hole, due to the presence of two cracks. As expected, the solutions rapidly converged at some characteristic crack length after one of the cracks was arrested. However, the difference in normalized stress intensity values can be significant in the vicinity of the hole at small crack lengths and could influence life predictions accordingly.

In addition to modeling open-hole specimens, specimen geometries posessing filled-holes (pins, bolts) with and without load transfer would normally be examined to evaluate the influence of these variables on the fatigue-crack-growth life of structural sub-components. This methodology is a typical "stepping stone" approach that adds additional levels of complexity to the fatigue-crack-growth life prediction process. This approach has been traditionally used when evaluating the robustness of life prediction tools as they are transitioned from research into real practice. Therefore in this study, reverse-dog-bone joint specimens were implemented as the next "step" of complexity, incorporating the effects of pin-loaded holes experiencing low-levels of load transfer. Eventually, this methodology would be extended to high load transfer bolted joints of increasing complexity (both single and multiple fastener patterns.)

The reverse-dog-bone geometry was a 0.25-inch-diameter hole, centered in a 1.5 inch-wide by 17-inch-long specimen, as shown in the finite element model of Figure A.3 (Appendix A). The purpose of modeling the reverse dog bone geometry was two-fold: First, an interference-fit pin condition was modeled to evaluate its effect on the localized stress distribution, in the crack plane, in the vicinity of the fastener hole. In previous studies, varying the level of interference has shown a significant effect on the fatigue lives of all types of joint configurations [8,9]. Another variable evaluated in these studies was the effect of bolt preload, which was not directly addressed during this effort. It was shown that the absence of strict criteria (drilling tolerances, bolt preload tolerances) during the manufacturing process had introduced variables that extended fatigue life and

produced significant scatter in the results. For example, it has been demonstrated that increasing the interference several mils (0.001 inches) will nearly triple the fatigue life of a joint, and varying a bolt preload will potentially double the fatigue life of a joint [8].

To account for the variability in interference level, the FRANC2D/L code was used to model one-half of the specimen geometry. One-half of the geometry was required due to the asymmetry of the specimen. The linear-elastic analysis represented the interference-fit pin by numerically expanding the pin in the fastener hole to some pre-defined value. In this study values ranging from 0.001 to 0.004-inch-diametric interference levels were examined to cover the variability in the specimen machining operation. In reality, a value of 0.001-inch-diametric interference would be more realistic due to the excessive amount of force required to install fasteners with diametric interferences greater than 0.001-0.002 inches.

Contact elements were used along the hole to simulate the hole-pin load interference. This model was adopted to determine the interference-fit pin's effect on the stress concentration, $\mathbf{K_t}$ ($\sigma_{max}/\sigma_{\infty}$) at the specimen's hole, allowing an adjustment to the assumed handbook value ($K_t \approx 3.1$) used by MODGRO [10]. This procedure allowed the applied stress ratio to be adjusted to account for a higher minimum "effective" stress introduced by the bolt-hole interference. This methodology was then incorporated to facilitate the prediction of fatigue-crack-growth lives using MODGRO. These life predictions were then calculated using a combination of MODGRO's load transfer model

and adjusted "effective" remote stress (σ_∞) to determine the interference-fit pin condition and its subsequent effect on the fatigue life.

Load transfer was at first assumed to be approximately 5%, as this value has been reported and/or assumed in previous studies involving the reverse-dog-bone specimens [8,11,12]. Calculations based on the reverse-dog-bone specimen configuration, using the "historical" method first reported by Sekhon et al. [11], also gave anticipated load transfer values of approximately 5.5%. However, test results (verified by FRANC2D/L models) had indicated that load transfer was more likely in the range of 0 to 0.5%. Therefore, two additional "clearance-fit" reverse-dog-bone specimens were tested, with the bolts loosened, to determine if any discrepancies existed between the calculated and actual fatigue life due to excessive bolt preloads and/or lack of load transfer. The experiment demonstrated that under full loading conditions the fasteners were able to rotate freely in their fastener holes, implying no relative movement between the joint components (no load transfer). Digital micrometers were used to check the clearance between the fastener and hole, before testing, to determine if the reverse-dog-bone specimens were "clearance-fit" specimens and not mistakenly "interference-fit" or cold-worked. The clearances were all within specifications and were approximately 0.001 inches. Therefore, life predictions made with the MODGRO program assumed both a filled-hole specimen configuration and no load transfer. Due to the long-term belief that 5-6% load transfer occurs in reverse-dog-bone specimens, it is suggested that additional

studies involving comprehensive test methods and multiple replicates be performed to verify the absence of load transfer in reverse-dog-bone specimens.

Secondly, a cold-worked condition was simulated in the reverse-dog-bone specimen geometry using the ANSYS$_{®}$ finite element program [13]. The ANSYS program was used because of its nonlinear geometric and material capabilities. A two-dimensional, nonlinear material, plane-stress (with thickness effects) approach was used. One-half of the specimen geometry was modeled, as before, and is shown in Figure A.3 (Appendix A). A very fine mesh was used in this task, in order to make comparative analyses between the FRANC2D/L and ANSYS models.

To model this situation, the hole was numerically expanded to a displacement representative of the cold-working process [14] and the residual stresses in the crack plane were calculated (Table B.2). This method has been previously reported to successfully estimate the residual stresses and strains in the vicinity of a cold-worked hole [15]. Actually, this model is a crude estimation of a rather complex process that in reality includes 3-D (thickness) variations in plasticity in vicinity of the hole, as well as asymmetry (asymmetric stress field) about the whole. These factors have been documented and verified using optical techniques using the same process used in this research [16].

The stresses obtained from the ANSYS finite element analysis were then implemented into MODGRO, using its "residual stress table" option, representing the cold-worked condition, thereby improving the life predictions of specimens with cold-worked fastener holes subjected to pin-loading (load transfer). This superposition method was first reported by Grandt [17], and has been shown to effectively account for the growth of cracks in residual stress fields [18]. A representation of the cold-worked stress field (von Mises stresses shown) can be found in Appendix A (Figure A.4).

The results of the ANSYS analysis for a 0.004-inch-diametric expansion is shown in Figure 2. Figure 2 contains the residual stresses (σ_x & σ_y) with respect to X-distance in the crack plane of the reverse-dog-bone specimen geometry. In our case, the residual stresses in the y-direction are of the most concern because they directly influence the mode I stress intensity factors (K_I) used in the life prediction calculations. Of primary concern are the large compressive stresses in the vicinity of the fastener hole. As before, the variations encountered in the machining operation can directly influence the amount of cold-working present in the vicinity of the hole. These variations can only be accounted for by strictly monitoring the specimen drilling/cold-working/reaming process at each stage in the machining operation and taking the representative measurements on a specimen by specimen basis. This method was not implemented within this research program, primarily due to cost, logistics, and time restrictions. It should also be noted that the alternative, previously described practice may not be representative of actual conditions occurring in manufacturing practice.

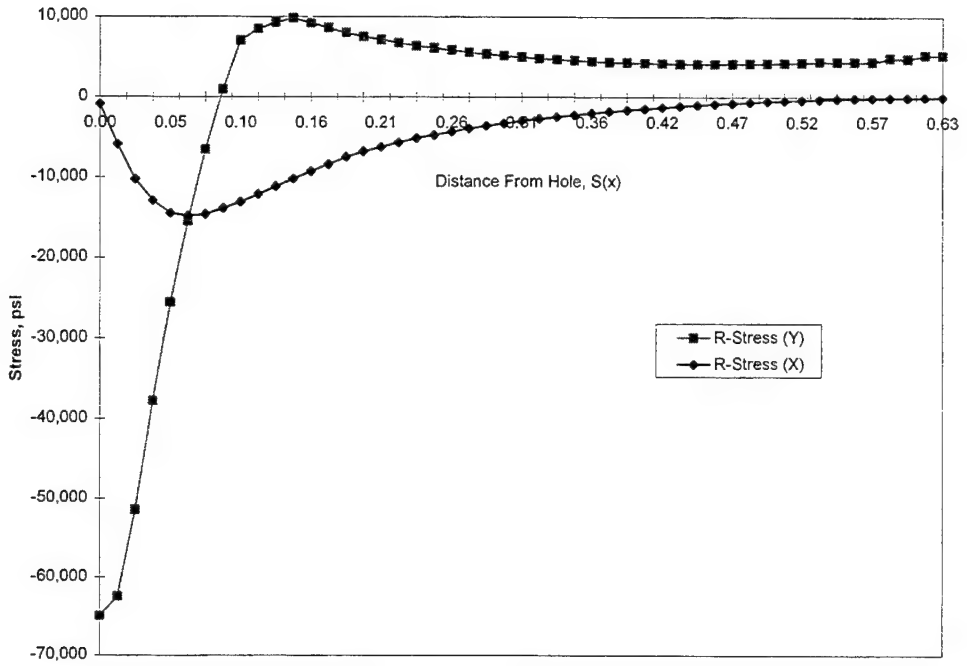

Figure 2 Residual Stress vs. Distance from Hole in Cold-worked Specimen

Therefore, it was decided that the residual stress fields in the vicinity of a cold-worked hole would be calculated for the "smallest" (0.001 inch) and "largest" (0.004 inch) diametric expansions using the ANSYS finite element program. It would be assumed that the life prediction results for the cold-worked specimens would incorporate residual stresses that would fall within this range of values. The variation in the y-direction residual stresses between the two cases is shown in Figure 3. Note the nonlinear unloading condition that occurs at large compressive stresses in excess of the material's yield strength (~57-65 ksi). Otherwise, this solution compares well with the "exact"

elastic-plastic solution obtained by Hsu and Forman [19]. (The Hsu-Forman solution does not consider nonlinear unloading).

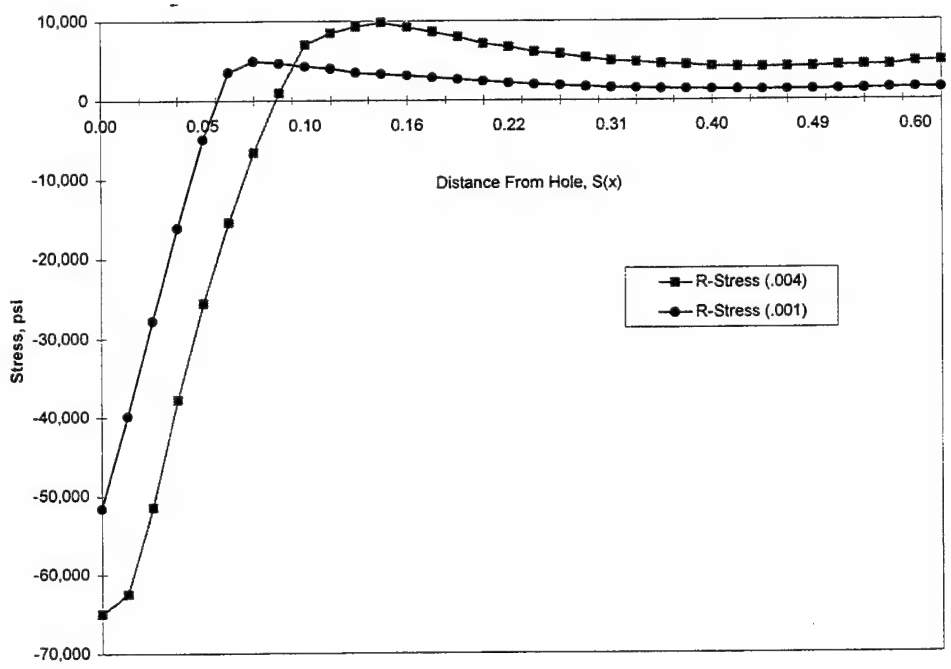

Figure 3 Variation in Residual Stresses (Y-dir) due to Cold-working

3.2. Life Predictions

In this task, the fatigue lives of the specimens tested under tasks 4 and 6 were analytically predicted using the MODGRO crack-growth life prediction software. These predictions were broken up into two parts, one for each specimen configuration. The life predictions

were generated without knowledge of the results of the verification tests. To predict fatigue-crack-growth results, three types of information were required: (1) the crack configuration (i.e., stress intensity factor), (2) the loading history, and (3) the baseline material property behavior (i.e. fatigue-crack-growth rate as a function of applied stress intensity factor range). All tests conducted under tasks 5, 6, 7, and 8 involved constant amplitude loading with a stress ratio (R) of 0.1. This type of loading did not require a closure or retardation model (or its associated parameters) for proper modeling and predictions.

The initial crack configuration for the flawed open-hole and flawed reverse-dog-bone tests was a corner crack with a surface length of 0.03 to 0.05 inches. The surface length was visually measured against a Mylar tape scale with 0.005 inch graduations using a microscope with a magnification of 40X. The initial crack length for the analysis was determined from surface measurements after pre-cracking. The initial crack shape was assumed to be semicircular with a crack depth equal to crack length. The US Air Force life prediction code, MODGRO, incorporates stress intensity factor solutions for numerous crack configurations, including the corner flaw assumed in these models. Additionally, MODGRO has the capability of predicting when the corner flaw has grown through the thickness of the specimen, and subsequently converting the stress intensity factor solution to that of a through-the-thickness crack propagating from an open-hole in a finite-width body [20,21,22].

The baseline material property data for 7075-T73 aluminum was obtained from Structural Integrity Branch in-house data, which served as the Structural Material Database. A comparison between the da/dN vs. ΔK data from the Air Force Design Data Handbook Database [23], the Structural Material Database and the flawed open-hole tests was made to determine if any differences in behavior existed. A comparison between the da/dN vs. ΔK data generated in this study and Structural Material Database is shown in Figure 4.

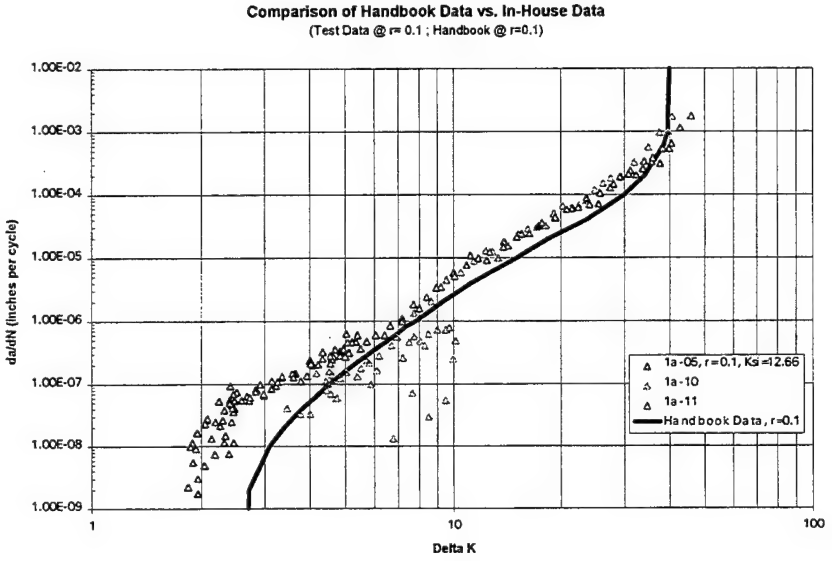

Figure 4 Comparison of Data from DO#1 & Structural Material Database

The data from the handbook represented the crack-growth behavior of 7075-T73 aluminum subjected to a stress ratio (R) of 0.1. The line plot of the handbook data should have fit the test data nicely, but discrepancies existed. Therefore, the handbook data were

corrected to reflect the actual test data for the 7075-T73 aluminum. The corrected handbook data are compared to the test data in Figure 5.

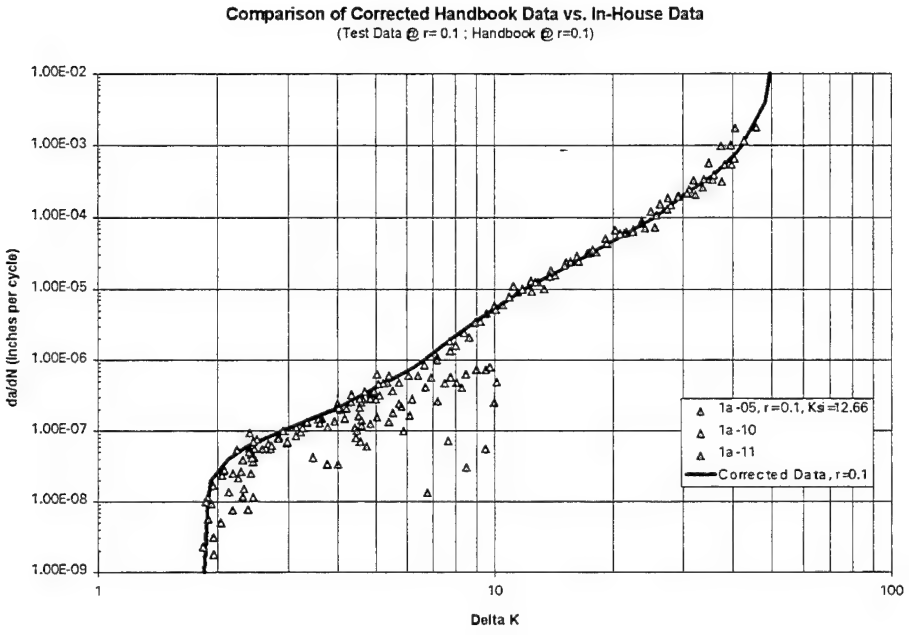

Figure 5 Graph Showing Improved Fit of Corrected Handbook Data

Using the corrected data, MODGRO was used to make the fatigue life predictions. The corrected data were incorporated into MODGRO's internal material database (matfile.dat) and life predictions were performed on Silicon Graphics workstations available within the Wright Laboratory Fatigue and Fracture Test Facility.

3.2.1. Life Predictions for Flawed Open-Hole Tests

The life predictions for the fatigue-crack-growth tests conducted in task 4 are shown in Figure 6. This figure shows the predictions using both the original and corrected handbook data normalized with respect to the actual life of each specimen. The actual life has also been included which, when normalized, yields the value of one.

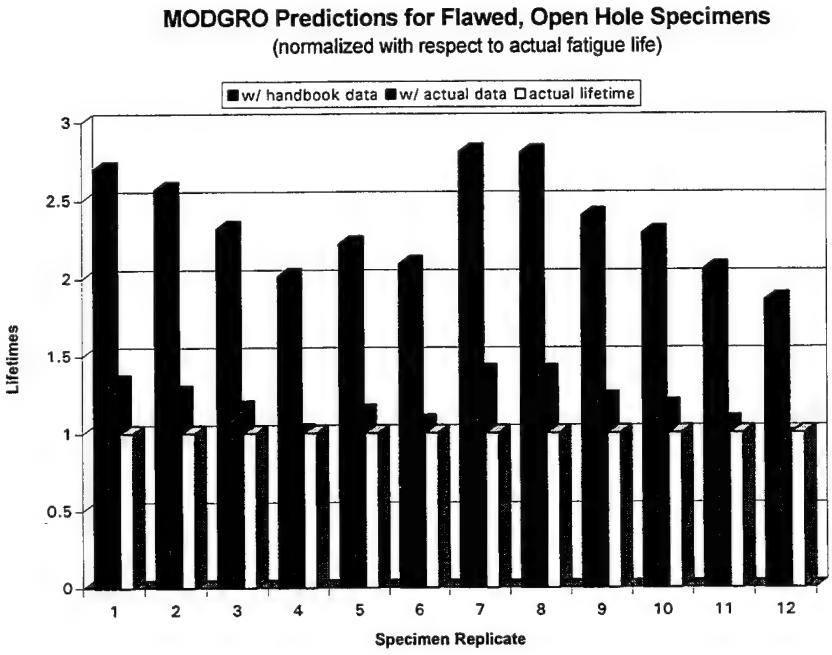

Figure 6 Improved Accuracy of MODGRO Predictions

The corrected data provided an improved life prediction capability using the MODGRO program. A table showing the plotted values is shown in Table 1.

Table 1 MODGRO Predictions vs. Open-Hole Test Data

				Predicted Failure		
Specimen #	Stress	PreCrack	Hole	Handbook	In-House	Actual
2a-12	16.20	0.039	0.255	123,982	60,932	45,969
2a-13		0.036	0.256	126,395	61,911	49,229
2a-14	18.23	0.036	0.255	84,865	42,468	36,634
2a-15		0.038	0.254	84,014	42,138	41,763
2a-16	22.28	0.046	0.254	40,926	20,870	18,452
2a-17		0.044	0.253	41,514	21,181	19,864
2b-12	16.17	0.041	0.253	105,092	52,173	37,440
2b-13		0.030	0.255	113,773	56,372	40,621
2b-14	18.28	0.035	0.251	73,240	37,137	30,555
2b-17		0.042	0.254	68,970	35,193	30,154
2b-18	22.50	0.041	0.250	35,103	18,182	17,084
2b-19		0.046	0.250	34,035	17,750	18,326

The average error in life predictions was approximately 18%, which is considered very reasonable. Typical sources of error would include: misinterpretations of the initial flaw shape, incorrect measurements of the initial hole diameters, manufacturing deviations (hole roundness, specimen width), fluctuations in loading due to controller/machine system interactions, scatter in crack-growth rate data, material nonhomogeneity, and other human factors. However, in this study, the presence of a second crack originating from the opposite side of the hole during fatigue cycling was perhaps the largest contributor to the discrepancies between predicted and actual fatigue-crack-growth life values.

For every open-hole specimen, a second crack was observed to originate and grow during fatigue cycling at approximately 2,000 to 12,000 cycles before failure. This occurrence

dramatically affected the fatigue-crack-growth rates in the open-hole specimens, causing them to fail earlier than originally predicted. In effect, the specimens behaved as a single crack specimen for a portion of the fatigue life, and behaved like an asymmetric, double cracked specimen for the remainder of the fatigue life. Also, since the constant amplitude fatigue life of double cracked specimens is much less than single cracked specimens, it should be expected that the actual fatigue life would be less than originally predicted. Because this type of behavior was consistently observed throughout this task, comparative values between single corner crack predictions, double corner crack predictions and actual fatigue life are listed below in Table 2.

Table 2 Comparison Between Single and Double Corner Crack Life Predictions

			PREDICTED FAILURE		
Specimen #	Stress	PreCrack	Single Crack	Double Crack	ACTUAL
2a-12	16.20	0.039	60,932	36,641	45,969
2a-13		0.036	61,911	37,686	49,229
2a-14	18.23	0.036	42,468	25,214	36,634
2a-15		0.038	42,138	27,728	41,763
2a-16	22.28	0.046	20,870	11,872	18,452
2a-17		0.044	21,181	12,096	19,864
2b-12	16.17	0.041	52,173	29,191	37,440
2b-13		0.030	56,372	33,094	40,621
2b-14	18.28	0.035	37,137	20,904	30,555
2b-17		0.042	35,193	19,299	30,154
2b-18	22.50	0.041	18,182	9,851	17,084
2b-19		0.046	17,750	9,480	18,326

It should be noted that when predicting the fatigue-crack-growth life of specimens (as well as structures) the "realistic" situation should be modeled. Failure to do so could lead to nonconservative life predictions and potentially dangerous situations. For example, if an individual was scheduling inspection intervals (for a similar situation) using MODGRO, it would be suggested to "bound" the problem by examining both cases and determining a conservative value for fatigue-crack-growth life. Interpolating between both cases could provide an adequate inspection interval if determined by knowledgeable personnel. On the other hand, the "conservative" double corner crack case could be used if an individual felt uncomfortable making engineering estimations.

Therefore, as was demonstrated in this study, the fatigue life predictions of single corner crack open-hole specimens will tend to approach either an "upper bound" (single corner crack) or "lower bound" (double corner crack) value based on how early (or late) the second crack initiates during in the fatigue-crack-growth life of the specimen. (The earlier a second crack initiates, the more likely its value will approach that of a double crack case.) Again, it is very important that the proper situation be modeled to generate safe, accurate life predictions.

3.2.2. Life Predictions for Flawed Reverse-Dog-Bone Specimens

This configuration includes both bearing and bypass loading of the hole. In addition, three types of pin loading were simulated: clearance-fit, interference-fit and cold-worked. As described previously, the stress state in the vicinity of the hole for the interference-fit and cold-worked pin cases was determined using the FRANC2D/L and ANSYS finite element analysis programs. Also, the FRANC2D/L code was also used to estimate percent load transfer applied to a pin-loaded hole possessing a crack through the specimen's thickness. The stress intensity factor for the corner crack configuration was approximated by superimposing the pin effects from the through-the-thickness analysis to that of an open-hole specimen with a corner crack, using MODGRO. After the analysis predicts that the corner crack has grown across the thickness, the through-the thickness stress intensity factor was used. The load history was constant amplitude with a stress ratio (R) of 0.1.

Initial results for the clearance-fit reverse-dog-bone specimens are shown below in Table 3. Reverse-dog-bone specimens were assembled by an outside manufacturing organization, so the fastener hole diameter for the specimens was assumed to be approximately 0.25 inches. It was also assumed, as described in Section 3.1, that no load transfer was present. Additionally, corner flaws were assumed to be semicircular in shape.

Table 3 MODGRO Predictions & Clearance-Fit RDB Specimens

Specimen #	Stress	PreCrack	Hole	Predicted Failure	Actual
3a-06	14.67	0.040	0.250	55,776	860,081
3a-07		0.034	0.250	60,807	111,841
3a-08		0.040	0.250	55,776	104,222

At first glance, the difference between predicted and actual failure seem quite disturbing. However, it was determined that there were three potential sources of error in addition to those mentioned in Section 3.2.1. These three variables were the effects of potential bolt and fastener hole interference, bolt preload (clamp-up), and time to failure between the flawed fastener hole and total specimen failure which was recorded in this report. A "clamp-up" force between the specimen layers, due to the bolt preload, can cause local stresses near the hole to redistribute and reduce the applied stress intensity, $\Delta \mathbf{K}$, by reducing the local stress gradient. Two of the variables (bolt-hole interference, bolt pre-loading) could occur during the manufacturing process and would be transparent to testing personnel.

To prove these assumptions, two additional clearance-fit reverse-dog-bone specimens were tested under the same conditions shown in Table 3. Both specimens had surface flaws approximately 0.04 inches long. However in these experiments, the fasteners were loosened to a "finger tight" condition to remove the effect of bolt preloading. Also, the time between failure of the flawed fastener hole (first) and total specimen failure (second)

was recorded. The effect of a potential interference-fit condition was assumed to be negligible. The flawed fastener holes in the two specimens failed at 57,471 cycles and 58,002 cycles, respectively. The times between the initial flawed fastener hole and total specimen failure were 7,118 cycles and 9,415 cycles, respectively. Upon further examination, this data would imply, along with the no-load transfer assumption, that the average error in life predictions was approximately 1.5%, which is exceptional. (In this study, the percent error was estimated as the difference between the calculated and actual fatigue lives, divided by the actual fatigue life and multiplied by 100.)

The results for the interference-fit reverse-dog-bone specimens are shown below in Table 4. As was described in Section 3.1, the variability in manufacturing parameters (amount of interference, bolt preloading) could only be accounted for by assuming a potential range of life predictions. This was determined to be a reasonable approach, for test evidence demonstrated that some reverse-dog-bone joints were subjected to high bolt pre-loads (specimen 3b-07 failed outside the test section, which is a commonly observed result of joint specimens with high bolt preloads). The amount of diametric interference was estimated to be between 0.001 inches and 0.004 inches and are shown below as "best" and "worst" case scenarios.

Table 4 MODGRO Predictions & Interference-Fit RDB Specimens

Specimen #	Stress	PreCrack	Hole	Predicted Failure 0.001 Int	0.004 Int	Actual
3b-06	14.67	0.062	0.250	68,591	156,892	239,221
3b-07		0.035	0.250	94,014	212,203	N/A
3b-08		0.033	0.250	97,296	218,305	378,600

Review of the results demonstrates that there is a synergistic effect between the level of interference and bolt preloading that occurred during testing. As the results show, the effect of interference alone would not be enough to explain the large discrepancies between the predicted and observed values. It is also apparent that further replicates should be tested under the conditions stated above, to demonstrate the influence of these variables on the fatigue life of interference-fit reverse-dog-bone specimens. In addition, the simplified remote stress altering approach used in this study (discussed in Section 3.1), could be replaced by first evaluating a finite element model of an interference-fit reverse-dog-bone specimen under loading and then inserting these values into the MODGRO "Beta Correction Table" or planned "User Input Beta Table" functionality.

The results for the cold-worked reverse-dog-bone specimens are shown below in Table 5. As mentioned in previous sections, the variability in manufacturing parameters (amount of cold-working, bolt preloading) could only be accounted for by assuming a potential range of life predictions. The amount of diametric cold-working was estimated to be between 0.001 inches and 0.004 inches and is shown below as "best" and "worst" case scenarios. The stress distributions were duplicated from the results of elastic-plastic

ANSYS finite element analyses, and input into MODGRO through the "Residual Stress Table" option. No potential fastener interference effects were expected, because the manufacturing tolerances for the "hole reaming" process were much tighter than in the other specimens, and final hole diameter was expected to be between 0.249 inches and 0.250 inches. Another potential source of error would be the amount of time between the initial flawed fastener hole failure and total specimen failure. This period would be increased in this case due to the interference-fit pin condition.

Table 5 MODGRO Predictions & Cold-Worked RDB Specimens

				Predicted Failure		
Specimen #	Stress	PreCrack	Hole	0.001 CW	0.004 CW	Actual
3c-06	14.67	0.099	0.250	355,357	None	452,010
3c-07		0.047	0.250	None	None	N/A
3c-08		0.046	0.250	None	None	N/A

A review of the results demonstrates that stress level was not high enough to grow cracks at surface crack lengths less than 0.05 inches. This case was true regardless of the amount of cold-working present in the specimens. This was demonstrated in both specimens 3c-06 and 3c-07, which ran over 4 million cycles separately without crack growth or failure. The only possible situation under which flaw growth could occur is under a limited cold-working and large surface flaw condition. In the one reported case the error was determined to be 21%, which is very reasonable. Potential sources of error have been previously mentioned in Section 3.1 and this section. The most significant would probably be the simplified assumption of a residual stress field being a two-

dimensional process and not accounting for the effects of bolt preloading. The amount of error due to the failure of the flawed first fastener hole and the total specimen failure would fall between the clearance-fit case and the interference-fit cases. This is because the second hole in the cold-worked reverse dog bone specimen was not cold-worked.

4. VERIFICATION TESTING

The verification testing involved four tasks. In tasks 4 and 5, flawed and unflawed open-hole specimens were tested, respectively. In tasks 6 and 7, flawed and unflawed reverse-dog-bone specimens were tested, respectively.

All verification testing was performed in the Fatigue & Fracture Test Facility, Bldg. 65, Area B, WPAFB. The 0.25-inch-thick open-hole and reverse-dog-bone specimens were tested in two 100-kip and one 50-kip MTS servo-hydraulic fatigue test frames using 20% and 50% load range settings respectively. These test frames are numbered 3, 4, and 10. The thin (0.09-inch-thick) specimens were tested in load frames using a load range of 20% (10% for the 4.5 kip maximum load) on 50-kip capacity frames. These test frames are numbered 12 and 13. All test frames were operated in load control with MTS 458 test controllers. Load control signals were generated with MS-DOS based computers running MATE software. A matrix describing these tasks is shown in Table 6.

Table 6 Fatigue Verification Test Matrix.

Task Number	Specimen Type	Max. Load (kips)	Frequency (Hz)	Flawed Specimens	Unflawed Specimens
4 and 5	Open-Hole 0.25 inch thick	16.0 18.0 22.0	10 10 10	2 2 2	4 2 2
4 and 5	Open-Hole 0.09 inch thick	5.75 6.5 8.0	10 10 10	2 4 2	4 5 2
6 and 7	Reverse Dog-Bone Clearance Fit	11.0	10	3	4
6 and 7	Reverse Dog-Bone Interference Fit	11.0	10	3	3
6 and 7	Reverse Dog-Bone Cold Worked	11.0	10	3	3

4.1. Flawed Open-Hole Tests

Fatigue-crack-growth rate tests were conducted on flawed, open-hole specimens of 7075-T73 aluminum. The tests were conducted under constant amplitude loading, and the environment was room temperature lab air. Corner cracks were introduced into the open-hole fatigue specimens by using a jeweler's saw to cut a 0.02 to 0.03 inch-long (and roughly the same length deep) notch to one side of a 0.1875-inch-diameter hole and normal to the direction of loading. The specimens were then subjected to fatigue loading

at 80% of the maximum loads given in Table 6 to initiate a crack from the notch. The cyclic loading was continued until the crack grew 0.06 to 0.08 inches beyond the hole. After pre-cracking, the specimen hole was redrilled to a diameter of 0.25 inches to remove the jeweler's saw notch and its potential effect on the local stress field. This process left a corner crack at one edge of the hole with a surface length of 0.03 to 0.05 inches. If the resulting corner-crack was insufficient, the pre-cracking process was continued until the crack reached the desired length.

Prior to testing, the specimen width, thickness, and initial surface crack length were measured and recorded. The specimens were tested under constant amplitude loading, at the loads specified in Table 6. During the fatigue testing, measurements of surface crack length were made as a function of applied fatigue cycles. The crack length readings were made at increments of less than 0.015 inches while the crack was still considered a corner crack, and at increments no greater than 0.15 inches after the crack became a through-the-thickness crack. Crack length measurements were made for any other cracks that formed during the test. Any anomalies observed during the test were noted.

The result of this task was an experimental record of crack length as a function of fatigue cycles for a corner crack propagating from an open hole in a finite width specimen of 7075-T73 aluminum. These records can be found in Appendix C.

4.2. Unflawed Open-Hole Tests

Nineteen specimens of 7075-T73 aluminum with unflawed, open holes were fatigued to failure. The tests were conducted under constant amplitude loading at the loads specified in Table 6, and the environment was room-temperature lab air. The number of cycles required to fail the specimen were recorded, and any anomalies observed during the test are noted.

The result of this task was an experimental record of the number of cycles required to fail the unflawed, open-hole 7075-T73 aluminum specimens, which is presented in Appendix C.

4.3. Flawed Reverse-Dog-Bone Tests

Fatigue-crack-growth tests were conducted on reverse-dog-bone joint specimens designed for low (5%) load transfer. Before testing, a corner flaw was initiated in one-half of the specimen assembly. The corner cracks were introduced into an open-hole of the fatigue specimens by using a jeweler's saw to cut a 0.02 to 0.03 inch-long (and roughly the same length deep) notch to one side of a 0.1875-inch-diameter hole. The notch plane was normal to the direction of loading. The specimens were pre-cracked at a stress level not exceeding 80% of the maximum stress applied during the fatigue testing. The fatigue

pre-cracking continued until the surface crack length was 0.04 to 0.05 inches beyond the hole. After fatigue pre-cracking, the specimen hole was redrilled to a diameter of 0.25 inches, as previously described. The pre-cracking was sufficient that after redrilling, only a small corner crack existed at the edge of one side of the hole. The specimens were then assembled with the crack exposed to a matching unflawed specimen to form a single reverse-dog-bone test specimen.

Prior to testing, measurements of specimen width, thickness, and initial surface crack length were made. The specimens were tested under constant amplitude loading, at the loads specified in Table 6 in room temperature lab air. The number of cycles required to fail the specimen were recorded and any anomalies observed during the test were noted.

The result of this task was an experimental record of the number of cycles required to fail the flawed reverse-dog-bone 7075-T73 aluminum specimens, which is presented in Appendix C.

4.4. Unflawed Reverse-Dog-Bone Tests

Unflawed, reverse-dog-bone fatigue tests were also conducted. The tests were conducted under constant amplitude loading at the loads specified in Table 6 in a room temperature,

laboratory air environment. The number of cycles required to fail the specimens were recorded and any anomalies observed during the testing were noted.

The result of this task was an experimental record of the number of cycles required to fail the unflawed reverse-dog-bone 7075-T73 aluminum specimens, which is presented in Appendix C.

5. GRAPHICAL USER INTERFACE FOR MODGRO

Graphical User Interfaces (GUI) are the contemporary software technology that is rapidly transforming the character-based application to user-friendly "point and click," menu-driven, widget-based systems, thus promoting technology transfer to industry. A portable, Graphical User Interface (GUI) system was developed for the MODGRO program. The GUI was developed on a Silicon Graphics workstation using X-Window/Motif libraries for the UNIX Operating System. All routines were programmed in the "C" computer language. GUI software development was performed at both the Fatigue and Fracture Facility, Bldg. 65, Area B, WPAFB, OH and AS&M, Inc., 107 Research Drive, Hampton, VA.

The graphical system is easily portable to any UNIX platform including SUN, HP, IBM, DEC. The GUI integrates the analytical capabilities of the MODGRO source code with graphical pre and postprocessing of data, thus offering complete visualization. This work was divided into three parts: (1) integration of menu buttons, (2) development of graphics capability, and (3) display of geometry and initial crack configurations. These topics are discussed in the following subsections.

This interface has been designed to be user-driven; the user no longer has to complete a predefined sequence of steps to perform a crack-growth analysis, but may select desired

options using pull-down menus and dialog boxes. The various graphical elements that comprise the interface are logically grouped, based on function, and are enclosed in separate windows. The primary "Specimen Configuration" window consists of a menu bar, a display area that contains a figure of the flaw configuration being analyzed, and other controls for manipulation of the figure (specimen configuration). A secondary "Status" window displays a scrollable list of the various parameters and control data that pertain to the current analysis. Any changes made by the user are immediately reflected in both windows, offering the user instant feedback and access to data values. The data are manipulated using menu options and dialog boxes which are described in the following subsections.

5.1. Menus and Dialogs for MODGRO

All previously existing menu choices were replaced with pull-down menus and pop-up dialog boxes. The options in the preprocessing menu include reading or creating the data files (specimen geometry and loading) interactively. The configuration and dimensions are displayed graphically in the primary window and all related model information is displayed in the status window, as shown in Figure 7.

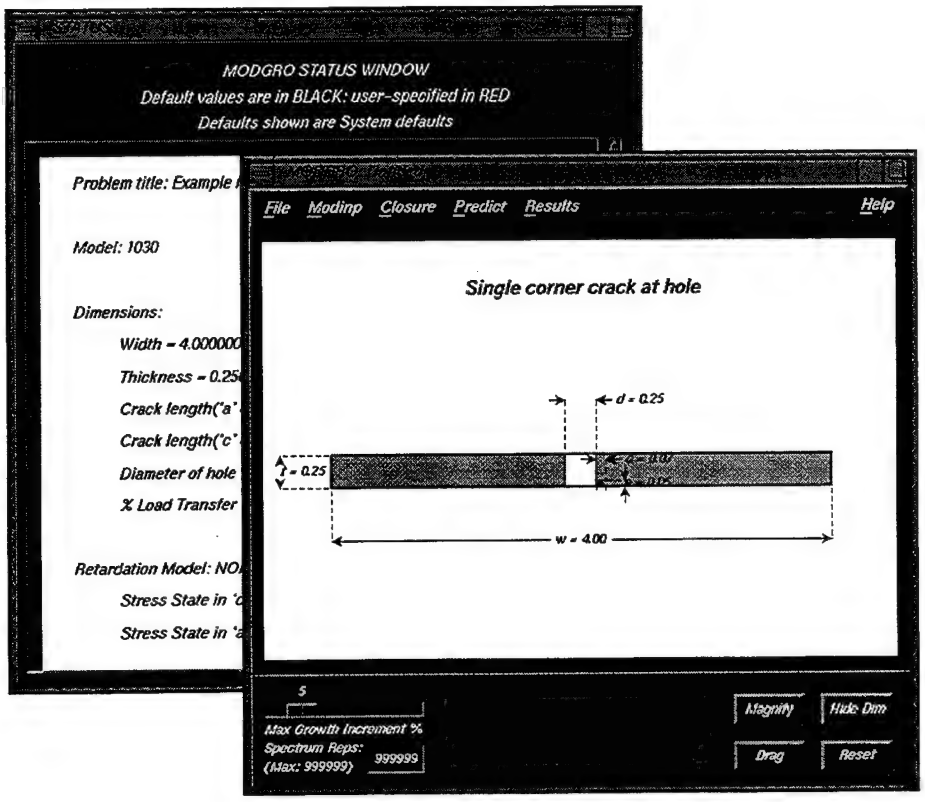

Figure 7 MODGRO Interface: Specimen Configuration and Status Windows

The title of the analysis can be changed by selecting the option under the preprocessing menu. A dialog box then prompts the user for a new title. Similarly, the material properties can be set by selecting the desired option under the material submenu. The material can be set from an existing material data file (tabular crack-growth rate data) or input by the user. An example of the tabular material data selection process is shown in Figure 8. Whenever required, dialog boxes pop up to request information from the user, to warn the user of potential errors, or to merely convey information to the user. The

dialogs function in a standardized manner, and by means of graphical or textual instruction, are extremely intuitive to the user.

Other parameters are set similarly by means of menu items and dialogs. Dialogs possess built-in error-checking functions to warn users of invalid data sets. They also have the capability to modify themselves in ways that guide the user through steps that could appear ambiguous under certain situations.

Execution of MODGRO is performed using menus and dialogs, similar to the pre-processing functions stated above.

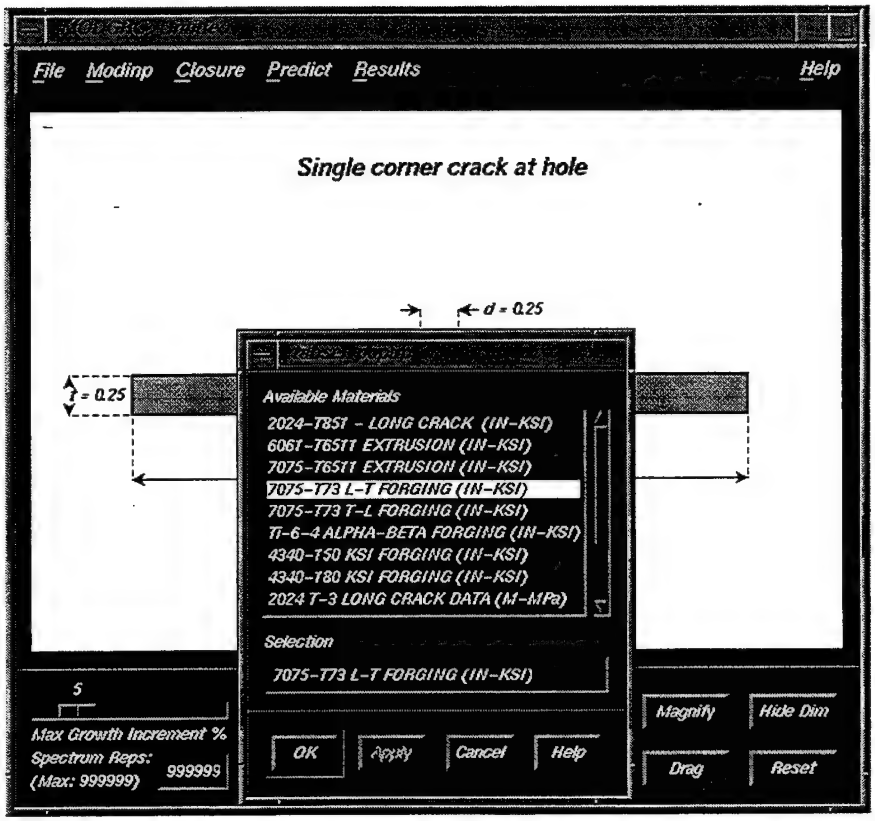

Figure 8 Example of MODGRO Tabular Material Data "Pop-up" Dialog

5.2. Graphical Display/Interactions of Specimen Configuration

In MODGRO's preprocessor, a figure of the analysis model, showing the specimen, initial crack configuration, location and dimensions are displayed in the primary window. Buttons to magnify or drag the model, and to turn the dimensioning on or off are integrated within the window. The model dimensions are updated and the model redrawn to the new scale when any of the dimensions are changed.

Load spectrums may also be viewed on the primary window. This feature will be further enhanced to allow for zooming and scaling of the spectrum.

The Status window displays all model data in an easy-to-read format. This feature enables the user to control the program by having access to all data values at any time. The display is color-coded within the Status window to indicate default and user-input values. The status window can be previewed in Figure 9.

Figure 9 MODGRO "Status" Window

A limited amount of on-line help was introduced into MODGRO. At this point in time, the on-line help feature was introduced to merely provide proof-of-concept. Invoking help will produce a window that contains detailed information about the help topic and diagrams illustrating examples. This window contains buttons to navigate through multiple help pages. Further development efforts will include a comprehensive help system for all menu items. An example of a "help" page can be seen in Figure 10.

5.3. Program Testing, Debugging and Maintenance

This GUI development effort included the testing and debugging of certain MODGRO functions. The code was modified to eliminate possible user-errors and to enhance fault-tolerance and robustness.

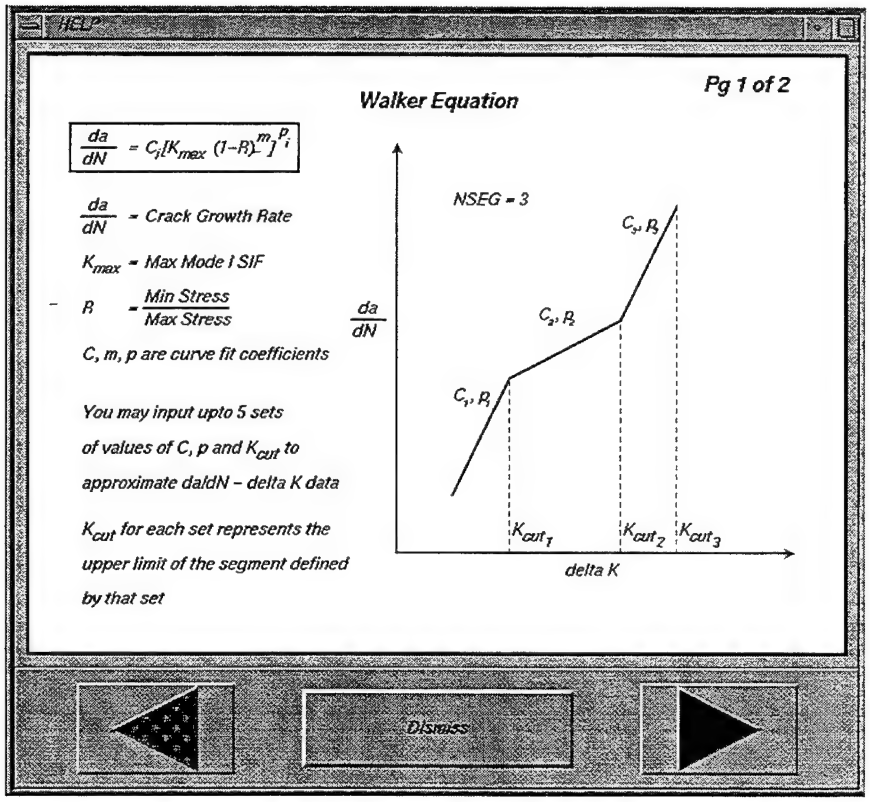

Figure 10 Example "Help" Page in MODGRO

6. REFERENCES

[1] Harter, J. A., "MODGRO User's Manual-Version 1.2," *AFWAL-TM-88-157-FIBE*, Air Force Flight Dynamics Laboratory, Wright-Patterson Air Force Base, OH, February 1988 (Revised February 1994).

[2] Wawrzynek, P. and Ingraffea, A.R., "Interactive Finite Element Analysis of Fracture Processes: An Integrated Approach," *Theoretical and Applied Fracture Mechanics*, Vol. 8, 1987, pp. 137-150.

[3] Wawrzynek, P. and Ingraffea, A.R., "An Edge-Based Data Structure for Two Dimensional Finite Element Analysis," *Engineering with Computers*, Vol. 3, 1987, pp. 13-20.

[4] Bowie, O.L., "Analysis of an Infinite Plate Containing Radial Cracks Originating from the Boundary of an Internal Circular Hole." *Journal of Mathematics and Physics*, Vol. 35, 1956, pp. 60-71.

[5] Paris, P.C. and Sih, G.C., "Stress Analysis of Cracks" Fracture Toughness Testing and It's Applications, *ASTM STP 381*, 1964, p. 70.

[6] Fedderson, C.F., "Finite Width Corrections," Plain Strain Crack Toughness Testing of High Strength Metallic Materials, *ASTM STP 410*, 1966, pp. 77-79.

[7] Grandt, A.F., Jr., "Lecture Notes on Linear Elastic Fracture Mechanics," School of Aeronautics and Astronautics, Purdue University, W. Lafayette, IN, 1995, p. 2-5.

[8] Urzi, R.B., "Standardization of Fastener Tests," Lockheed-California Company, *Report No. LR 24328*, December 1970.

[9] Moore, T.K., "The Influence of Hole Processing & Joint Variables on the Fracture Life of Shear Joints," *AFML-TR-77-167*, Ait Force Materials Laboratory, Wright-Patterson Air Force Base, OH, Vol. 1, February 1978.

[10] Peterson, R.E., "Stress Concentration Factors for Tension Stressing of a Finite Width Plate," *Stress Concentration Factors*, John Wiley & Sons, Inc., 1974, p. 150.

[11] Sekhon, J.S., Duncan, W.E., Ecker, L.F., "An Evaluation of Test Methods for Fastened Assemblies," *Assembly Engineering*, Vol. 12, No. 9, September 1969.

[12] Tiffany C.F., Stewart, R.P., Moore, T.K., "Fatigue and Stress-Corrosion Test of Selected Fasteners/Hole Processes," *ASD-TR-72-111*, Aeronautical Systems Division, Wright-Patterson Air Force Base, OH, January 1973.

[13] *ANSYS User's Manual, Vol. I-Procedures*, Swanson Analysis Systems, Inc., P.O. Box 65 Johnson Road, Houston, PA, 1992, pp. 3-135 to 3-138.

[14] Landy, M.A., "Cold Expansion of Fastener and Other Holes Using the Split Sleeve System (Cx) and Countersink Cold Expansion Nosecap (CsCx),", *FTI Engineering Process Specification FTI 8101B*, Fatigue Technology, Inc., 100 Andover Park West, Seattle, WA, 1984.

[15] Adler, W.F., Dupree, D.M., "Stress Analysis of Cold-worked Fastener Holes." *AFML-TR-74-44*, Air Force Materials Laboratory, Wright-Patterson Air Force Base, OH, July 1974.

[16] Sanford, R.J., Graham, S.M., Link, R.E., "The Mechanics of Cold Expanded Fastener Holes in 7075-T651 Aluminum," *Final Report NASC Contract No. N00019-83C-0305*, Naval Air Systems Command, Washington, D.C., October 1986.

[17] Grandt, A.F., Jr.,"Stress Intensity Factors for Some Through-Cracked Fastener Holes." *International Journal of Fracture*, Vol. 11, No. 2, April 1975, pp 283-294.

[18] Cathey, W.H., Grandt, A.F. Jr., "Fracture Mechanics Consideration of Residual Stresses Introduced by Cold-working Fastener Holes," *Journal of Engineering Materials and Technology*, Vol. 102, January 1980, pp. 85-91.

[19] Hsu, Y.C., and Forman, R.G., "Elastic-Plastic Analysis of an Infinite Sheet Having a Circular Hole Under Pressure," *ASME Journal of Applied Mechanics*, Vol. 42, No. 2, 1975, pp. 347-352.

[20] Snow, J.R., "A Stress Intensity Factor Calibration for Corner Flaws at an Open Hole," *AFML-TR-74-282*, Air Force Materials Laboratory, Wright-Patterson Air Force Base, OH, 1975.

[21] Grandt, A.F., Jr.,and Macha, D.E., "Digitized Measurements of the Shape of Corner Cracks at Fastener Holes," *Engineering Fracture Mechanics*, Vol. 17, No. 1, 1983, pp. 63-73.

[22] Grandt, A.F., Jr., Harter, J.A., and Heath, B.J., "The Transition of Part-Through Cracks at Holes into Through-the-Thickness Flaws," Fracture Mechanics: Fifteenth Symposium, *ASTM STP 833*, 1984, pp. 7-23.

[23] Skinn, D.A, Gallagher, J.P., Berens, A.P., Huber, P.B., Smith, J., "Damage Tolerant Design Handbook," *WL-TR-94-4055*, Air Force Materials Directorate, Wright-Patterson Air Force Base, OH, Vol. 4, Chapter 8, May 1994.

APPENDIX A

Figure A.1: FRANC2D/L Model of Open-Hole Specimen Geometry

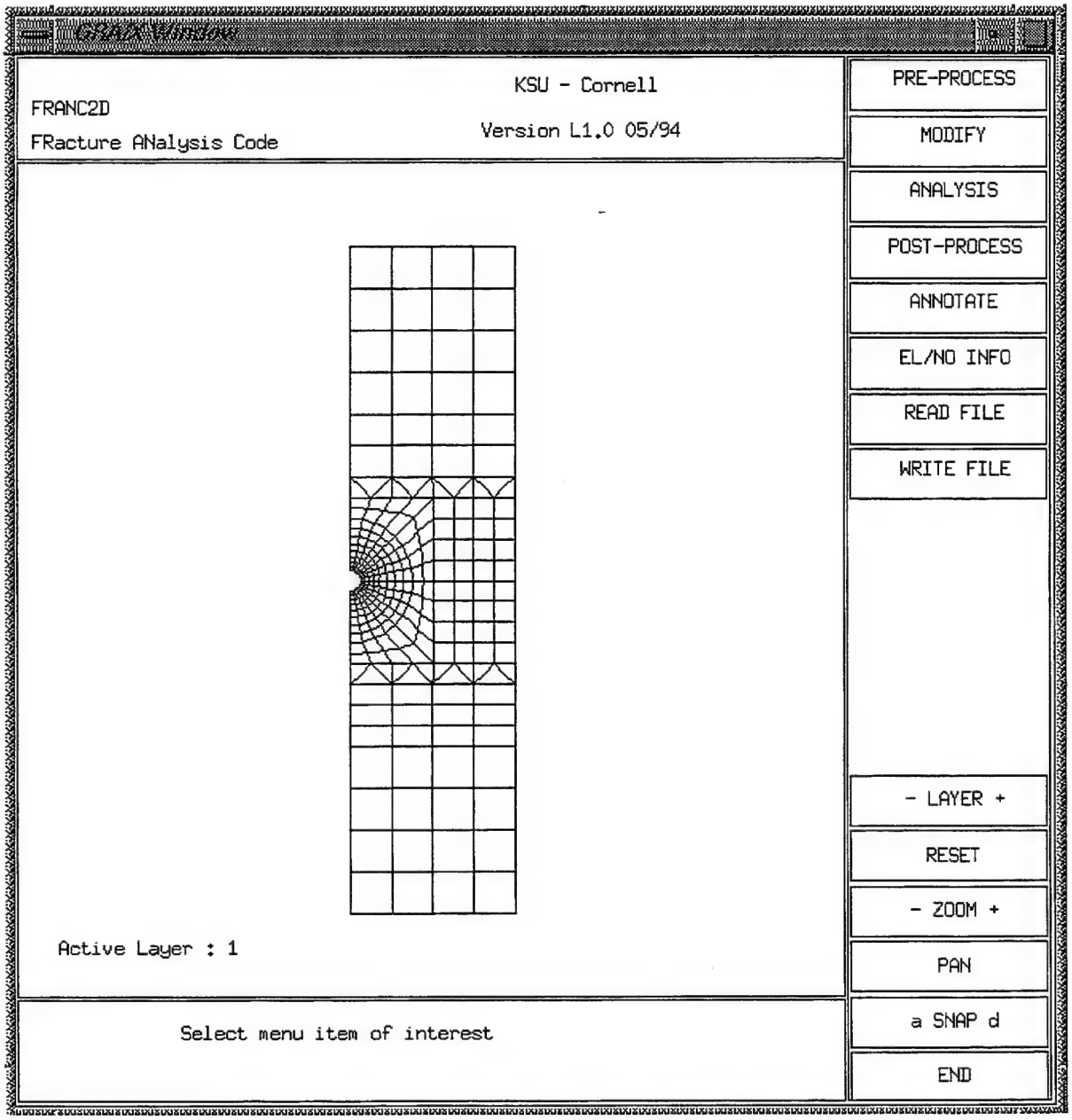

Figure A.2: Open-Hole Specimen Crack Configuration (+/-45^0)

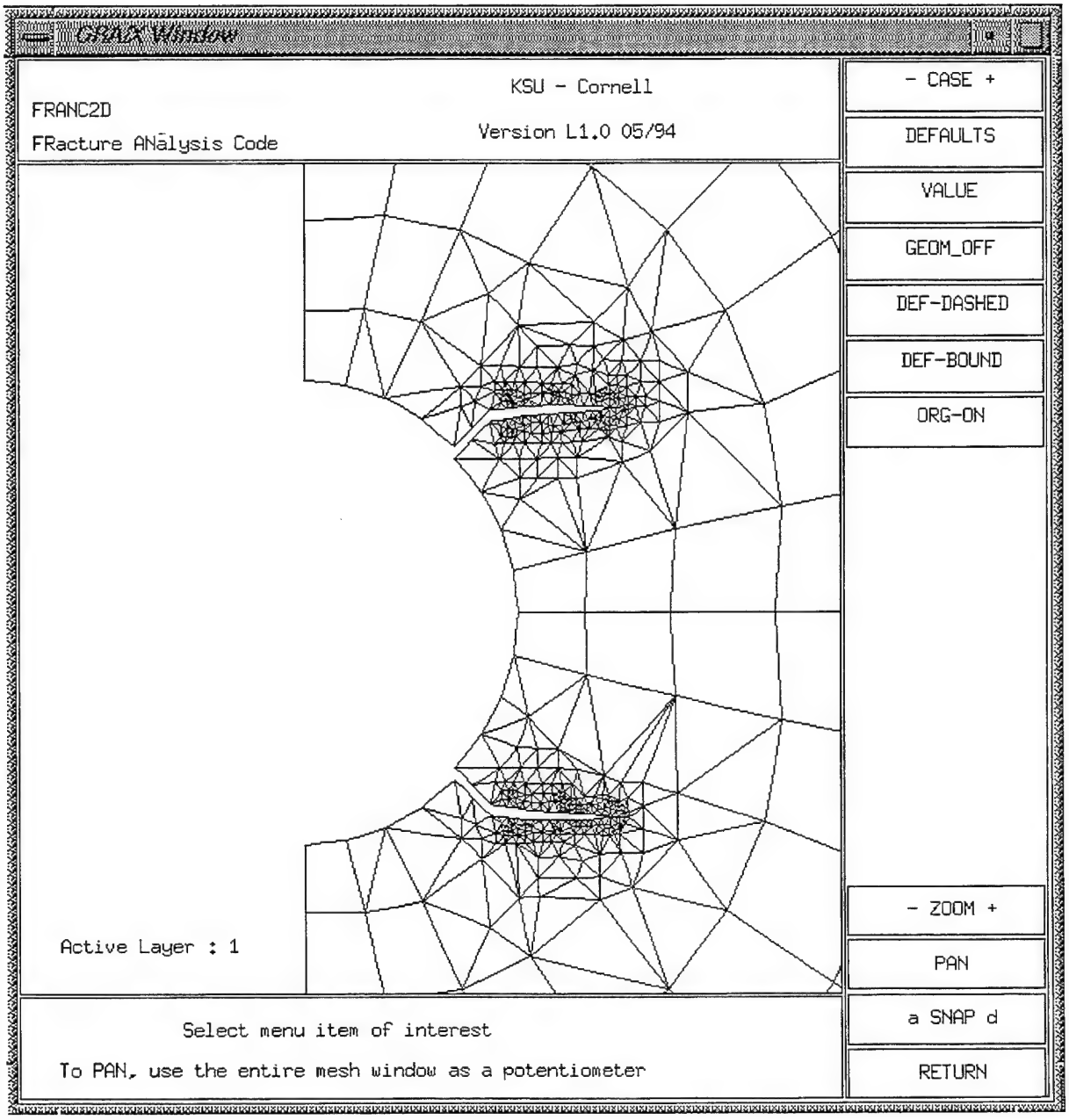

Figure A.3: ANSYS Model of Reverse-Dog-Bone Specimen Geometry

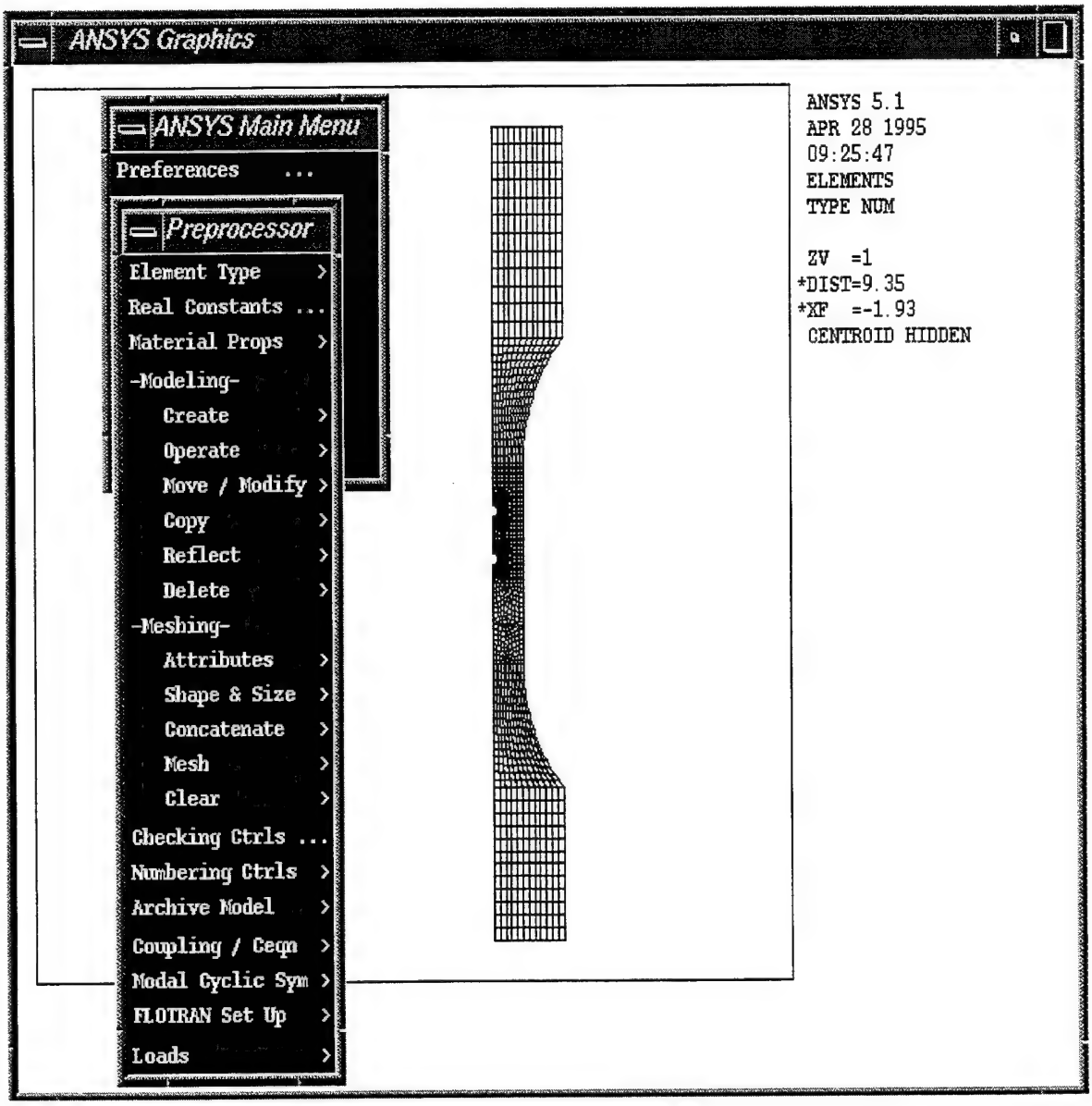

Figure A.4: Reverse-Dog-Bone Specimen Residual Stress Field

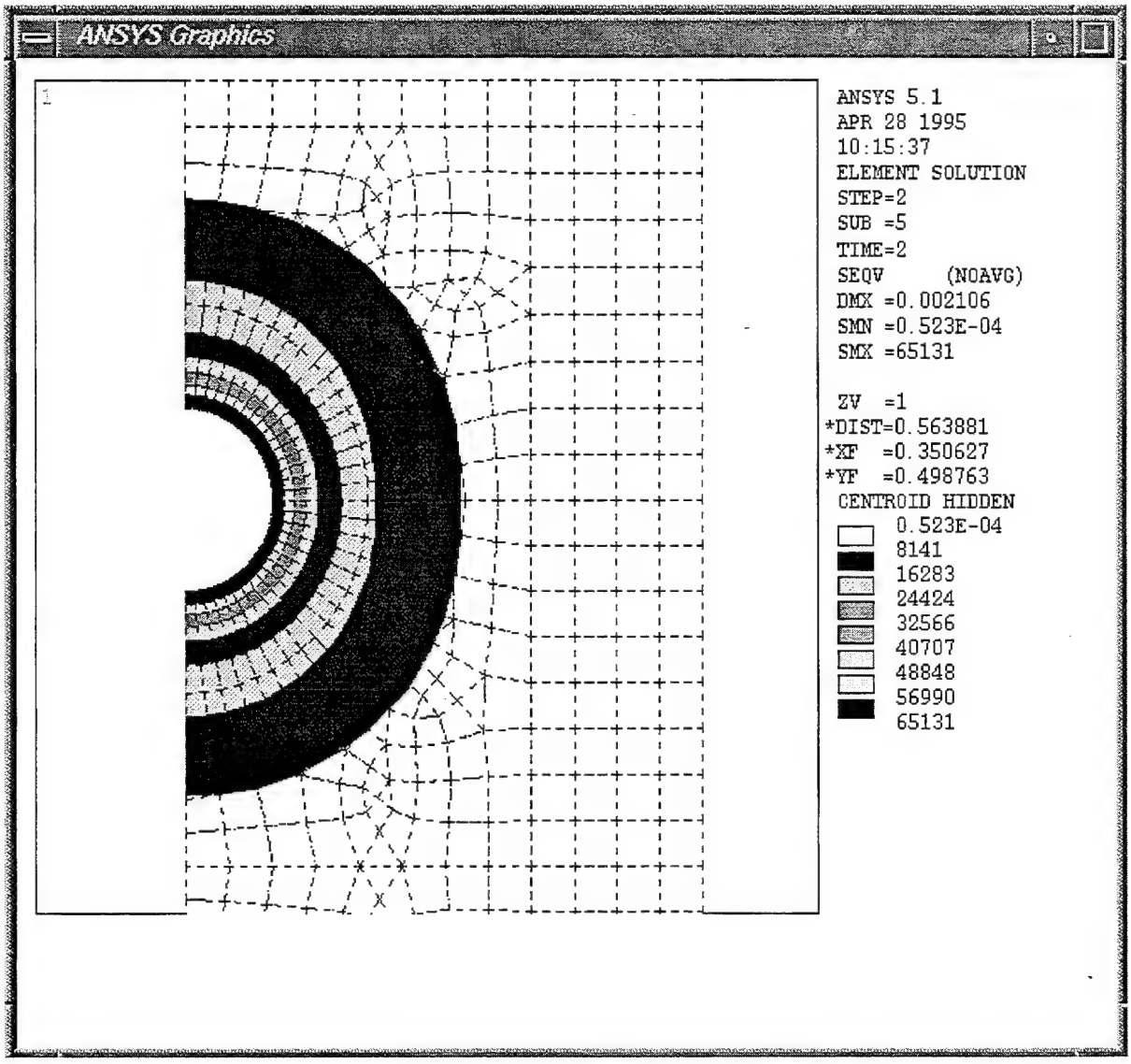

APPENDIX B

Table B.1: FRANC2D/L FEA Crack-Growth Data

Table B.2: ANSYS FEA Residual Stress Data

Table B.1: FRANC2D/L FEA Crack-Growth Data

FRANC2D Results From Four Cracks (+/-45 degrees) in an Open Hole Specimen

X	Y	C	KI	KII	Nrm SIF (KI)	Nrm SIF (KII)
0.1096	0.1096	0.03	0.2736	0.1241	0.8912	0.4042
0.1195	0.1108	0.04	0.4062	-0.0023	1.1459	-0.0064
0.1294	0.1121	0.05	0.4630	0.0121	1.1682	0.0306
0.1394	0.1129	0.06	0.5098	0.0062	1.1742	0.0144
0.1494	0.1134	0.07	0.5446	0.0078	1.1613	0.0166
0.1594	0.1137	0.08	0.5764	0.0038	1.1498	0.0075
0.1694	0.1139	0.09	0.5987	0.0003	1.1260	0.0006
0.1794	0.1139	0.10	0.6139	0.0020	1.0953	0.0036
0.1894	0.1140	0.11	0.6314	-0.0012	1.0740	-0.0020
0.1994	0.1141	0.12	0.6470	-0.0077	1.0538	-0.0126
0.2094	0.1144	0.13	0.6781	0.0082	1.0610	0.0128
0.2194	0.1145	0.14	0.7170	0.0047	1.0811	0.0071
0.2294	0.1145	0.15	0.7553	0.0065	1.1003	0.0095
0.2394	0.1143	0.16	0.7902	0.0009	1.1146	0.0013
0.2494	0.1141	0.17	0.8214	0.0096	1.1240	0.0132
0.2594	0.1136	0.18	0.8530	0.0025	1.1343	0.0033
0.2693	0.1131	0.19	0.8875	0.0076	1.1487	0.0098
0.2793	0.1124	0.20	0.9204	0.0023	1.1612	0.0029
0.2893	0.1116	0.21	0.9460	0.0042	1.1647	0.0052
0.2993	0.1108	0.22	0.9760	0.0046	1.1740	0.0055
0.3093	0.1099	0.23	1.0013	0.0049	1.1780	0.0057
0.3192	0.1089	0.24	1.0270	-0.0001	1.1827	-0.0001
0.3291	0.1078	0.25	1.0520	0.0052	1.1871	0.0059
0.3390	0.1067	0.26	1.0700	0.0012	1.1839	0.0014
0.3490	0.1056	0.27	1.0890	0.0023	1.1824	0.0025
0.3589	0.1044	0.28	1.1110	-0.0015	1.1846	-0.0016
0.3688	0.1032	0.29	1.1250	0.0000	1.1786	0.0000
0.3788	0.1020	0.30	1.1490	0.0032	1.1835	0.0032
0.3887	0.1009	0.31	1.1640	-0.0038	1.1795	-0.0039
0.3986	0.0996	0.32	1.1760	0.0060	1.1729	0.0060
0.4085	0.0983	0.33	1.2030	-0.0003	1.1815	-0.0003
0.4184	0.0970	0.34	1.2180	-0.0020	1.1785	-0.0020
0.4284	0.0957	0.35	1.2370	-0.0021	1.1797	-0.0020
0.4383	0.0945	0.36	1.2490	0.0023	1.1745	0.0021
0.4482	0.0932	0.37	1.2610	-0.0018	1.1696	-0.0016
0.4581	0.0919	0.38	1.2710	-0.0015	1.1633	-0.0014
0.4681	0.0907	0.39	1.2950	0.0030	1.1699	0.0027
0.4780	0.0894	0.40	1.3116	-0.0053	1.1700	-0.0048
0.4879	0.0883	0.41	1.3250	-0.0057	1.1675	-0.0050
0.4978	0.0872	0.42	1.3390	-0.0032	1.1657	-0.0028
0.5078	0.0861	0.43	1.3550	-0.0012	1.1658	-0.0010
0.5177	0.0851	0.44	1.3760	0.0011	1.1704	0.0009
0.5277	0.0840	0.45	1.3830	-0.0022	1.1632	-0.0019
0.5376	0.0830	0.46	1.3990	-0.0028	1.1638	-0.0023

0.5476	0.0820	0.47	1.4090	-0.0041	1.1595	-0.0034
0.5576	0.0811	0.48	1.4270	0.0012	1.1621	0.0010
0.5675	0.0802	0.49	1.4370	0.0003	1.1582	0.0002
0.5774	0.0792	0.50	1.4554	-0.0019	1.1612	-0.0015
0.5874	0.0783	0.51	1.4650	-0.0155	1.1574	-0.0123
0.5974	0.0776	0.52	1.4770	-0.0006	1.1556	-0.0005
0.6074	0.0769	0.53	1.4900	0.0028	1.1547	0.0021
0.6173	0.0762	0.54	1.5120	-0.0012	1.1609	-0.0009
0.6273	0.0755	0.55	1.5280	0.0058	1.1624	0.0044
0.6373	0.0747	0.56	1.5410	-0.0099	1.1618	-0.0075
0.6473	0.0740	0.57	1.5474	-0.0064	1.1563	-0.0048
0.6572	0.0734	0.58	1.5618	0.0016	1.1570	0.0012
0.6672	0.0728	0.59	1.5820	0.0007	1.1620	0.0005
0.6772	0.0722	0.60	1.5950	-0.0040	1.1617	-0.0029
0.6872	0.0717	0.61	1.6060	-0.0017	1.1601	-0.0012
0.6972	0.0711	0.62	1.6190	0.0004	1.1600	0.0003
0.7071	0.0706	0.63	1.6340	-0.0074	1.1615	-0.0053
0.7171	0.0702	0.64	1.6520	0.0048	1.1651	0.0034
0.7271	0.0696	0.65	1.6670	-0.0039	1.1666	-0.0027
0.7371	0.0692	0.66	1.6820	0.0001	1.1681	0.0001
0.7471	0.0687	0.67	1.7060	0.0056	1.1759	0.0039
0.7571	0.0682	0.68	1.7180	-0.0106	1.1754	-0.0072
0.7671	0.0068	0.69	1.7330	0.0039	1.1771	0.0026
0.7771	0.0674	0.70	1.7420	-0.0035	1.1747	-0.0023
0.7871	0.0670	0.71	1.7620	-0.0055	1.1798	-0.0037
0.7971	0.0666	0.72	1.7750	-0.0010	1.1802	-0.0007
0.8071	0.0663	0.73	1.7910	0.0035	1.1827	0.0023
0.8171	0.0659	0.74	1.7960	-0.0023	1.1779	-0.0015
0.8271	0.0656	0.75	1.8250	0.0023	1.1889	0.0015
0.8370	0.0652	0.76	1.8400	-0.0028	1.1908	-0.0018
0.8470	0.0649	0.77	1.8560	0.0007	1.1933	0.0005
0.8570	0.0645	0.78	1.8700	-0.0012	1.1946	-0.0008
0.8670	0.0642	0.79	1.8790	-0.0014	1.1927	-0.0009
0.8770	0.0639	0.80	1.9010	0.0004	1.1991	0.0002
0.8870	0.0635	0.81	1.9070	0.0008	1.1955	0.0005
0.8970	0.0632	0.82	1.9260	-0.0015	1.2000	-0.0009
0.9070	0.0629	0.83	1.9377	-0.0062	1.2000	-0.0038
0.9170	0.0627	0.84	1.9460	-0.0026	1.1979	-0.0016
0.9270	0.0624	0.85	1.9609	0.0059	1.2000	0.0036
0.9370	0.0621	0.86	1.9872	-0.0075	1.2090	-0.0046
0.9470	0.0619	0.87	2.0117	0.0080	1.2168	0.0048
0.9570	0.0617	0.88	2.0235	-0.0024	1.2170	-0.0015
0.9670	0.0614	0.89	2.0433	0.0001	1.2220	0.0001
0.9770	0.0611	0.90	2.0615	-0.0051	1.2260	-0.0031
0.9870	0.0609	0.91	2.0700	0.0023	1.2243	0.0014
0.9970	0.0607	0.92	2.0996	-0.0080	1.2350	-0.0047
1.0070	0.0605	0.93	2.1178	0.0073	1.2390	0.0043
1.0170	0.0603	0.94	2.1380	-0.0019	1.2441	-0.0011
1.0270	0.0601	0.95	2.1610	-0.0013	1.2509	-0.0007
1.0370	0.0599	0.96	2.1899	-0.0035	1.2610	-0.0020
1.0470	0.0597	0.97	2.2083	0.0066	1.2650	0.0038

1.0570	0.0595	0.98	2.2250	0.0083	1.2681	0.0047
1.0670	0.0592	0.99	2.2468	-0.0085	1.2740	-0.0048
1.0770	0.0590	1.00	2.2652	0.0002	1.2780	0.0001
1.0870	0.0587	1.01	2.2850	0.0015	1.2828	0.0008
1.0970	0.0585	1.02	2.3230	-0.0095	1.2977	-0.0053
1.1070	0.0583	1.03	2.3300	0.0024	1.2953	0.0013
1.1170	0.0582	1.04	2.3580	0.0009	1.3045	0.0005
1.1269	0.0590	1.05	2.3774	0.0020	1.3090	0.0011
1.1369	0.0577	1.06	2.4110	-0.0048	1.3212	-0.0026
1.1469	0.0576	1.07	2.4280	-0.0034	1.3243	-0.0018
1.1569	0.0575	1.08	2.4450	-0.0015	1.3274	-0.0008
1.1669	0.0574	1.09	2.4810	0.0136	1.3407	0.0073
1.1769	0.0571	1.10	2.4966	-0.0155	1.3430	-0.0084
1.1869	0.0570	1.11	2.5260	0.0107	1.3527	0.0057
1.1969	0.0568	1.12	2.5529	-0.0088	1.3610	-0.0047
1.2069	0.0567	1.13	2.5900	0.0034	1.3746	0.0018
1.2169	0.0566	1.14	2.6140	0.0019	1.3813	0.0010
1.2269	0.0564	1.15	2.6400	-0.0021	1.3889	-0.0011
1.2369	0.0562	1.16	2.6550	0.0011	1.3908	0.0006
1.2469	0.0561	1.17	2.6860	-0.0051	1.4010	-0.0027
1.2569	0.0560	1.18	2.7190	-0.0013	1.4122	-0.0007
1.2669	0.0559	1.19	2.7380	0.0111	1.4161	0.0058
1.2769	0.0557	1.20	2.7650	-0.0156	1.4241	-0.0081
1.2869	0.0556	1.21	2.7940	-0.0013	1.4330	-0.0006
1.2969	0.0555	1.22	2.8350	0.0083	1.4481	0.0043
1.3069	0.0554	1.23	2.8550	-0.0025	1.4524	-0.0013
1.3169	0.0553	1.24	2.8890	-0.0003	1.4637	-0.0002
1.3269	0.0552	1.25	2.9210	0.0019	1.4740	0.0010
1.3369	0.0551	1.26	2.9540	-0.0078	1.4847	-0.0039
1.3469	0.0549	1.27	2.9880	0.0101	1.4959	0.0050
1.3569	0.0548	1.28	3.0120	-0.0041	1.5020	-0.0020
1.3669	0.0547	1.29	3.0510	-0.0039	1.5156	-0.0019
1.3769	0.0547	1.30	3.0790	0.0011	1.5236	0.0006
1.3869	0.0546	1.31	3.1126	0.0021	1.5343	0.0010
1.3969	0.0545	1.32	3.1544	-0.0049	1.5490	-0.0024
1.4069	0.0544	1.33	3.1930	0.0036	1.5621	0.0018
1.4169	0.0543	1.34	3.2370	-0.0039	1.5777	-0.0019
1.4269	0.0542	1.35	3.2740	0.0030	1.5898	0.0015
1.4369	0.0541	1.36	3.3110	-0.0060	1.6018	-0.0029
1.4469	0.0541	1.37	3.3463	-0.0001	1.6130	-0.0001
1.4569	0.0539	1.38	3.3870	0.0075	1.6267	0.0036
1.4669	0.0539	1.39	3.4350	-0.0090	1.6438	-0.0043
1.4769	0.0539	1.40	3.4760	0.0001	1.6575	0.0000
1.4869	0.0538	1.41	3.5250	0.0083	1.6748	0.0039
1.4969	0.0537	1.42	3.5737	-0.0079	1.6920	-0.0038
1.5069	0.0537	1.43	3.6140	0.0012	1.7051	0.0006
1.5169	0.0536	1.44	3.6620	0.0018	1.7217	0.0008
1.5269	0.0536	1.45	3.7094	-0.0029	1.7380	-0.0014
1.5369	0.0535	1.46	3.7608	0.0053	1.7560	0.0025
1.5469	0.0534	1.47	3.8145	-0.0019	1.7750	-0.0009
1.5569	0.0534	1.48	3.8705	0.0043	1.7950	0.0020

1.5669	0.0533	1.49	3.9312	-0.0065	1.8170	-0.0030
1.5769	0.0531	1.50	3.9921	0.0041	1.8390	0.0019

Arrested crack data:

X	Y	C	KI	KII	Nrm SIF (KI)	Nrm SIF (KII)
0.1096	-0.1096	0.03	0.2744	-0.1244	0.8938	-0.4052
0.1195	-0.1108	0.04	0.4050	-0.0021	1.1425	-0.0061
0.1294	-0.1121	0.05	0.4642	-0.0125	1.1712	-0.0314
0.1394	-0.1129	0.06	0.5083	-0.0050	1.1708	-0.0115
0.1494	-0.1135	0.07	0.5469	-0.0146	1.1662	-0.0312
0.1594	-0.1135	0.08	0.5790	-0.0042	1.1549	-0.0084
0.1694	-0.1137	0.09	0.5993	-0.0002	1.1271	-0.0004
0.1794	-0.1139	0.10	0.6152	-0.0052	1.0976	-0.0093
0.1894	-0.1139	0.11	0.6347	-0.0115	1.0797	-0.0196
0.1994	-0.1143	0.12	0.6511	-0.0009	1.0604	-0.0015

Table B.2: ANSYS FEA Residual Stress Data

Summary Data from Ansys Cold-Worked Case (4 mil expansion)
X-distance (S) from Hole versus σ_x and σ_y
(Distance measured in Crack Plane)

Distance (S)	σ_x (psi)	σ_y (psi)
0.00000	-854.18	-64,983.00
0.01302	-5,868.20	-62,466.00
0.02604	-10,203.00	-51,438.00
0.03906	-12,885.00	-37,773.00
0.05208	-14,432.00	-25,545.00
0.06510	-14,767.00	-15,447.00
0.07813	-14,606.00	-6,543.90
0.09115	-13,867.00	968.94
0.10417	-13,075.00	7,047.40
0.11719	-12,101.00	8,164.10
0.13021	-11,127.00	9,280.80
0.14323	-10,176.00	9,822.90
0.15625	-9,271.10	9,218.00
0.16927	-8,365.90	8,613.00
0.18229	-7,460.70	8,008.10
0.19531	-6,765.20	7,535.20
0.20833	-6,209.60	7,150.40
0.22135	-5,653.90	6,765.60
0.23437	-5,111.50	6,390.90
0.24740	-4,706.80	6,122.90
0.26042	-4,302.10	5,854.90
0.27344	-3,897.40	5,586.80
0.28646	-3,548.40	5,364.20
0.29948	-3,251.50	5,183.90
0.31250	-2,954.50	5,003.60
0.32552	-2,657.50	4,823.40
0.33854	-2,424.90	4,700.80
0.35156	-2,200.40	4,585.50
0.36458	-1,975.90	4,470.20
0.37760	-1,763.10	4,367.50
0.39062	-1,597.60	4,315.70
0.40365	-1,432.00	4,263.80
0.41667	-1,266.40	4,212.00
0.42969	-1,100.90	4,160.10
0.44721	-956.07	4,134.70
0.45573	-842.37	4,148.80
0.46875	-728.67	4,163.00
0.48177	-614.97	4,177.10
0.49479	-501.27	4,191.20
0.50781	-412.50	4,245.70
0.52083	-340.36	4,327.10
0.53385	-268.22	4,408.50
0.54688	-196.07	4,489.90

0.55990	-123.93	4,571.30
0.57292	-87.89	4,721.60
0.58594	-60.87	4,889.20
0.59896	-33.85	5,056.70
0.61198	-6.83	5,224.20
0.62500	20.19	5,391.70

APPENDIX C

Test Data for Flawed Open-Hole Specimens

Test Data for Unflawed Open-Hole Specimens

Test Data for Flawed Reverse-Dog-Bone Specimens

Test Data for Unflawed Reverse-Dog-Bone Specimens

Test Data for Flawed Open-Hole Specimens

ID: 3-0-2A-12 (w=3.95"; t=0.25";
Al 7075-T7351 hole=0.255")

Left	Right	Crack-L	Crack-R	Cycles
8.146	8.440	0.000	0.039	0
8.146	8.510	0.000	0.109	10002
8.146	8.534	0.000	0.133	12005
8.146	8.550	0.000	0.149	13705
8.146	8.566	0.000	0.165	15309
8.146	8.581	0.000	0.180	16813
8.146	8.601	0.000	0.200	18315
8.146	8.795	0.000	0.394	28318
8.146	9.044	0.000	0.643	35821
8.146	9.141	0.000	0.740	38325
8.141	9.259	0.005	0.858	40827
8.136	9.345	0.010	0.944	42131
8.130	9.442	0.016	1.041	43331
8.079	9.650	0.067	1.249	45026
8.035	9.789	0.111	1.388	45629
8.010	9.856	0.136	1.455	45831
Failure	***	***	***	45969

ID: 3-0-2A-13 (w=3.95; t=0.25";
Al 7075-T7351 hole=0.256")

Left	Right	Crack-L	Crack-R	Cycles
7.954	8.246	0.000	0.036	0
7.954	8.302	0.000	0.092	10003
7.954	8.330	0.000	0.120	12005
7.954	8.344	0.000	0.134	13706
7.954	8.356	0.000	0.146	15308
7.954	8.371	0.000	0.161	17309
7.954	8.395	0.000	0.185	19311
7.954	8.625	0.000	0.415	32314
7.954	8.890	0.000	0.680	40816
7.948	8.986	0.006	0.776	43319
7.881	9.100	0.073	0.890	45821
7.641	9.315	0.313	1.105	48323
Failure	***	***	***	49229

ID: 3-0-2A-14 (w=3.95"; t=0.25";
Al 7075-T7351 hole=0.255")

Left	Right	Crack-L	Crack-R	Cycles
8.044	8.335	0.000	0.036	0
8.044	8.380	0.000	0.081	5003
8.044	8.413	0.000	0.114	7505
8.044	8.441	0.000	0.142	9509
8.044	8.470	0.000	0.171	11411
8.044	8.500	0.000	0.201	13113
8.044	8.585	0.000	0.286	18117
8.044	8.685	0.000	0.386	23120
8.044	8.816	0.000	0.517	28123
8.036	9.058	0.008	0.759	33125
Failure	***	***	***	36634

ID: 3-0-2A-15 (w=3.95"; t=0.25";
Al 7075-T7351 hole=0.254")

Left	Right	Crack-L	Crack-R	Cycles
7.452	7.744	0.000	0.038	0
7.452	7.783	0.000	0.077	5002
7.452	7.811	0.000	0.105	7505
7.452	7.837	0.000	0.131	9509
7.452	7.861	0.000	0.155	11411
7.452	7.882	0.000	0.176	13115
7.452	7.952	0.000	0.246	18118
7.452	8.026	0.000	0.320	23120
7.452	8.120	0.000	0.414	28123
7.448	8.317	0.004	0.611	35126
Failure	***	***	***	41763

ID: 3-0-2A-16 (w=3.95"; t=0.25";
Al 7075-T7351 hole=0.254")

Left	Right	Crack-L	Crack-R	Cycles
7.950	8.250	0.000	0.046	0
7.950	8.266	0.000	0.062	1003
7.950	8.285	0.000	0.081	2005
7.950	8.305	0.000	0.101	3008
7.950	8.325	0.000	0.121	4012
7.950	8.345	0.000	0.141	5016
7.950	8.365	0.000	0.161	6019
7.950	8.390	0.000	0.186	7023
7.950	8.447	0.000	0.243	9025
7.950	8.508	0.000	0.304	11029
7.950	8.640	0.000	0.436	14031
7.905	8.881	0.045	0.677	17033
Failure	***	***	***	18452

ID: 3-0-2A-17 (w=3.95"; t=0.25";
Al 7075-T7351 hole=0.253")

Left	Right	Crack-L	Crack-R	Cycles
7.346	7.643	0.000	0.044	0
7.346	7.659	0.000	0.060	1002
7.346	7.675	0.000	0.076	2005
7.346	7.692	0.000	0.093	3008
7.346	7.711	0.000	0.112	4010
7.346	7.730	0.000	0.131	5014
7.346	7.749	0.000	0.150	6017
7.346	7.770	0.000	0.171	7019
7.346	7.845	0.000	0.246	9020
7.346	7.875	0.000	0.276	11021
7.346	7.979	0.000	0.380	14023
7.346	8.116	0.000	0.517	17026
7.180	8.283	0.166	0.684	18520
7.141	8.330	0.205	0.731	18723
7.104	8.365	0.242	0.766	18926
7.053	8.416	0.293	0.817	19129
6.995	8.474	0.351	0.875	19332
6.924	8.551	0.422	0.952	19534
6.785	8.684	0.561	1.085	19737
Failure	***	***	***	19864

ID: 4-0-2b-12 (w=3.95"; t=0.09";
Al 7075-T73 hole=0.253")

Left	Right	Crack-L	Crack-R	Cycles
1.807	2.101	0.000	0.041	0
1.807	2.235	0.000	0.175	10002
1.807	2.267	0.000	0.207	12003
1.807	2.441	0.000	0.381	21004
1.807	2.655	0.000	0.595	28806
1.604	2.891	0.203	0.831	33808
1.445	3.037	0.362	0.977	35509
1.294	3.164	0.513	1.104	36512
1.074	3.370	0.733	1.310	37215
Failure	***	***	***	37440

ID: 4-0-2B-13 (w=3.95"; t=0.09";
Al 7075-T73 hole=0.255")

Left	Right	Crack-L	Crack-R	Cycles
5.550	5.835	0.000	0.030	0
5.550	5.928	0.000	0.123	10004
5.550	5.955	0.000	0.150	12006
5.550	6.094	0.000	0.289	21008
5.550	6.270	0.000	0.465	28810
5.437	6.506	0.113	0.701	35313
5.318	6.634	0.232	0.829	37316
5.239	6.724	0.311	0.919	38319
5.101	6.907	0.449	1.102	39622
4.956	7.144	0.594	1.339	40425
4.907	7.261	0.643	1.456	40577
Failure	***	***	***	40621

ID: 4-0-2b-14 (w=3.95"; t=0.09";
Al 7075-T73 hole=0.251")

Left	Right	Crack-L	Crack-R	Cycles
1.748	2.034	0.000	0.035	0
1.748	2.041	0.000	0.042	1504
1.748	2.052	0.000	0.053	3008
1.748	2.151	0.000	0.152	8010
1.748	2.225	0.000	0.226	13013
1.748	2.354	0.000	0.355	18015
1.748	2.526	0.000	0.527	23018
1.592	2.785	0.156	0.786	28021
1.148	3.281	0.600	1.282	30424
1.087	3.385	0.661	1.386	30527
Failure	***	***	***	30555

ID: 4-0-2b-17 (w=3.95"; t=0.09";
Al 7075-T73 hole=0.254")

Left	Right	Crack-L	Crack-R	Cycles
5.446	5.742	0.000	0.042	0
5.446	5.755	0.000	0.055	1504
5.446	5.766	0.000	0.066	3008
5.446	5.851	0.000	0.151	8011
5.446	5.953	0.000	0.253	13014
5.446	6.085	0.000	0.385	18017
5.446	6.270	0.000	0.570	23019
5.315	6.555	0.131	0.855	28022
Failure	***	***	***	30154

ID: 4-0-2B-18 (w=3.95"; t=0.09";
Al 7075-T73 hole=0.250")

Left	Right	Crack-L	Crack-R	Cycles
1.844	2.135	0.000	0.041	0
1.844	2.175	0.000	0.081	2004
1.844	2.199	0.000	0.105	3006
1.844	2.220	0.000	0.126	3760
1.844	2.246	0.000	0.152	4761
1.844	2.277	0.000	0.183	5762
1.844	2.310	0.000	0.216	6764
1.844	2.346	0.000	0.252	7766
1.844	2.381	0.000	0.287	8767
1.844	2.470	0.000	0.376	10770
1.844	2.577	0.000	0.483	12772
1.844	2.649	0.000	0.555	13773
1.659	2.812	0.185	0.718	15276
1.545	2.894	0.299	0.800	15778
1.357	3.024	0.487	0.930	16280
Failure	***	***	***	16684

ID: 4-0-2B-19 (w=3.95"; t=0.09";
Al 7075-T73 hole=0.250")

Left	Right	Crack-L	Crack-R	Cycles
5.554	5.850	0.000	0.046	0
5.554	5.868	0.000	0.064	2002
5.554	5.895	0.000	0.091	3006
5.554	5.911	0.000	0.107	3759
5.554	5.940	0.000	0.136	4763
5.554	5.970	0.000	0.166	5767
5.554	6.000	0.000	0.196	6770
5.554	6.037	0.000	0.233	7772
5.554	6.076	0.000	0.272	8776
5.554	6.161	0.000	0.357	10779
5.554	6.274	0.000	0.470	12781
5.554	6.338	0.000	0.534	13785
5.544	6.459	0.010	0.655	15289
5.540	6.506	0.014	0.702	15791
5.530	6.556	0.024	0.752	16293
5.510	6.610	0.044	0.806	16796
5.308	6.800	0.246	0.996	17800
4.959	7.094	0.595	1.290	18304
Failure	***	***	***	18326

Test Data for Unflawed Open-Hole Specimens

Specimen #	Stress	Hole	Failure @
2a-01	**	0.248	164,471
2a-02	**	0.248	Runout[1]
2a-03	16.20	0.248	115,187
2a-08		0.248	99,319
2a-04	18.23	0.248	85,509
2a-05		0.248	73,795
2a-06	22.28	0.248	32,955
2a-07		0.248	32,300
2b-01	16.17	0.248	290,041
2b-02		0.248	Failed in Grip
2b-08		0.248	Runout
2b-09		0.250	Runout
2b-03	18.28	0.248	Runout
2b-04		0.248	410,084
2b-07		0.248	Runout
2b-10		0.250	131,647
2b-11		0.250	98,901
2b-05	22.50	0.248	53,927
2b-06		0.248	36,770

**Test began at 14.18 ksi and was increased to 16.2 ksi when the specimen reached 1 Million Cycles of fatigue life w/no sign of damage

[1] runout constitutes 3 Million Cycles

Test Data for Flawed Reverse-Dog-Bone Specimens

Specimen #	Stress (kips)	PreCrack (inches)	Hole (inches)	Failure @ (cycles)	
3a-06	14.67	0.040	0.250	860081*	Failed Outside of Test Section
3a-09		0.034	0.250	111,841	
3a-08		0.040	0.250	104,222	
3b-06	14.67	0.062	0.250	239,221	
3b-07		0.035	0.250	795001*	Failed Outside of Test Section
3b-08		0.033	0.250	378,600	
3c-06	14.67	0.099	0.250	452,010	
3c-07		0.047	0.250	Runout	
3c-08		0.046	0.250	Runout	

Test Data for Unflawed Reverse-Dog-Bone Specimens

Specimen #	Stress (kips)	Failure @ (cycles)
3a-01	14.67	803,306
3a-02		123,533
3a-03		160,626
3a-04		398,526
3b-01	14.67	196,857
3b-02		398,870
3b-03		229,414
3c-01	16.67	314,900
3c-02		510,561
3c-03	14.67	791,698
3c-04		522,908
3c-05		812,378